Received: 28 April 2020 | Revised: 19 September 2020 | Accepted: 4 November 2020

DOI: 10.1111/jmg.12581

ORIGINAL ARTICLE

Journal of METAMORPHIC GEOLOGY WILEY

Metapelite from the high- to ultrahigh-pressure terrane of the Eastern Alps (Pohorje Mountains, Slovenia)—New pressure, temperature and time constraints on a polymetamorphic rock

Botao Li[1,2] | **Hans-Joachim Massonne**[1,2] | **Friedrich Koller**[3] | **Junfeng Zhang**[1]

[1]State Key Laboratory of Geological Processes and Mineral Resources, School of Earth Sciences, China University of Geosciences, Wuhan, China

[2]Fakultät Chemie, Universität Stuttgart, Stuttgart, Germany

[3]Geozentrum, Universität Wien, Wien, Austria

Correspondence
Hans-Joachim Massonne, State Key Laboratory of Geological Processes and Mineral Resources, School of Earth Sciences, China University of Geosciences, Lumo Road 388, 430074, Wuhan, China.
Email: h-j.massonne@mineralogie.uni-stuttgart.de

Funding information
MOST Special Fund from the State Key Laboratory of GPMR and the 111 Project (BP0719022); National Natural Science Foundation of China, Grant/Award Number: 42002068

Handling Editor: Simon Harley

Abstract

The Austroalpine nappe stack of the Pohorje Mountains (Mts.) in northeastern Slovenia comprises a suite of eclogite facies metamorphic rocks that were partially assigned to Eo-Alpine ultrahigh-pressure metamorphism (UHPM). We selected a micaschist, which was previously related to this metamorphism, for a detailed study including the chemical zonation of garnet and potassic white mica, the identification of mineral inclusion assemblages, pseudosection modelling with PERPLE_X, and monazite in-situ dating with the electron microprobe. Polymetamorphism was revealed by (at least) two generations of garnet and phengite and four populations of monazite yielding ages of 283.6 ± 6.1 (2σ), 94.1 ± 3.7, 47.9 ± 10.8 and 26.2 ± 2.8 Ma. The Permian monazite population is characterized by relatively high Y contents (~1.15 wt% Y) and low La/Gd mass ratios (8.7) indicating its formation before the growth of porphyroblastic garnet. The Eo-Alpine population, however, grew synchronously with garnet based on low Y contents (~0.05 wt%) and high La/Gd ratios (21.4). The older Tertiary population (48 Ma) shows also high Y contents (1.1 wt%) and low La/Gd ratios (10.6) whereas the younger Tertiary population is characterized by low Y contents. The Permian *P–T* conditions of 7.5–10 kbar at 600–650°C were obtained using the inclusion assemblage of staurolite+rutile+biotite in porphyroblastic garnet. High pressure (HP) but no UHPM was reconstructed for both Eo-Alpine coarse phengite (Si = 3.22 per formula unit = pfu) and small Tertiary garnet+fine-grained phengite (Si = 3.27 pfu) at peak pressures ~16 kbar and 18.5–23 kbar respectively. Maximum temperatures close to 650°C were likely reached during the Eo-Alpine HP event, whereas those of the Tertiary HP event were probably ~580°C. These HP metamorphic events suggest that the Pohorje Mts. experienced both an Eo-Alpine and a Tertiary subduction–exhumation history, the latter of which was mainly reported for underlying Penninic nappes so far.

KEYWORDS

high-*P* metapelite, monazite dating, Pohorje Mountains, *P–T* pseudosection, Zr-in-rutile geothermometry

1 | INTRODUCTION

The European Alps are one of the best studied orogens on our planet. Ideas on the evolution of continent–continent collisional orogens were developed based on studies of rocks from the European Alps. This is also true for the concept of deep subduction of continental material (e.g. Michard et al., 1993) as the first coesite-bearing rock of continental affinity was found in the Western Alps by Chopin (1984). Soon after Chopin's find, further ultrahigh-pressure (UHP) metamorphic rocks, characterized by coesite or at least pressure–temperature (*P–T*) conditions of the coesite stability field (see Massonne, 1999), were detected in the Dora-Maira Massif and other regions of the Western Alps (e.g. Compagnoni & Rolfo, 2003; Reinecke, 1998). It took much longer time until a first report of an UHP rock from the Eastern Alps came out (Janák et al., 2004). This rock, an eclogite, was sampled in the southeasternmost part of the Eastern Alps, the Pohorje Mountains (Mts.). A UHP rock of continental affinity, a metasediment rich in garnet and white mica (micaschist), followed since Janák et al. (2015) reported microdiamonds enclosed in garnet of this Pohorje rock.

The assignment of the southern Pohorje to an UHP terrane, which is, so far, unique in the Eastern Alps, depends on the reliability of the peak *P–T* estimates of 30–40 kbar at 700–940°C for UHP eclogite and micaschist and adjacent garnet peridotite (Hauzenberger et al., 2016; Janák et al., 2004, 2006, 2015; Vrabec et al., 2012). Recently, a maximum of only 24 kbar at ~700°C was estimated for peak pressures of micaschists from the southern Pohorje by Herg and Stüwe (2018). In addition, Miller and Konzett (2005) doubted that UHP metamorphic conditions for eclogite were ever reached arguing that the presence of coesite, not identified by microbeam techniques, is doubtful and other observations and/or thermodynamic calculations are indirect and, thus, insufficient to prove UHP conditions. The maximum *P–T* conditions of only 18–25 kbar and 630–750°C, determined for eclogite from the Pohorje by Miller et al. (2005) and Sassi et al. (2004), are consistent with the *P–T* estimates by Herg and Stüwe (2018) for micaschist and the common view that both rock types had experienced the same *P–T* conditions (see also Hurai et al., 2010; Janák et al., 2009; Krenn et al., 2009).

The above outlined discrepancies in peak pressures for eclogite and micaschist from the southern Pohorje motivated us to re-investigate such rocks. We focused first on the micaschist because only retrograde *P–T* paths were, so far, derived for this rock type. Our study questions the UHP nature of the micaschist. Instead, we provide evidence for three metamorphic events. The oldest event at medium pressures was followed by two different high pressure (HP) events. According to results obtained from in-situ dating of monazite, these events could be assigned to a late Permian, Eo-Alpine, and Tertiary metamorphism. As a consequence, the studied polymetamorphic micaschist sheds new light on geotectonic models for the southeastern part of the Eastern Alps.

2 | GEOLOGICAL SETTING

The Alpine orogen in Europe started to form in the Cretaceous due to the collision of the Adriatic continental upper plate with a subducting lower plate including Mesozoic and Tertiary oceans and the European passive continental margin (Dal Piaz et al., 2003). Two Alpine HP–UHP metamorphic events are well known, and are of Tertiary and Late Cretaceous (Eo-Alpine) age (Neubauer et al., 2000; Schmid et al., 2004). In addition, some metamorphic rocks of the Alpine events also underwent Variscan and late Permian orogenic cycles (e.g. Kirst et al., 2010; Schuster et al., 2001; Schuster & Stüwe, 2008; Thöni, 2003, 2006).

Traditionally, the Alps are subdivided into four major domains (Figure 1): the Penninic, Austroalpine and Helvetic zones and the Southern Alps (Dal Piaz et al., 2003). The Austroalpine is broadly exposed in the Eastern Alps and represents the core of the eastern Alpine belt (e.g. Fodor et al., 2008; Figure 1a,b). The Austroalpine nappe stack can be subdivided from bottom to top into the thrust sheets of the Lower Austroalpine, the Lower Central Austroalpine and the Upper Central Austroalpine (e.g. Janák et al., 2004). The region of the Pohorje Mts. in northeastern Slovenia is located at the southeastern margin of the Eastern Alps north of the Periadriatic Line, and was related to the Central Austroalpine basement (Figure 1b). In terms of large-scale tectonics, the Pohorje area is made up of a nappe stack, which consists of three tectonic units (Hauzenberger et al., 2016). The lower unit is termed Pohorje nappe, which belongs to the Lower Central Austroalpine according to Janák et al. (2006). This unit consists of micaschist, gneiss and amphibolite with lenses of marble, quartzite, eclogite and ultramafic rocks (Figure 1c). The mafic and ultramafic rocks show oceanic affinity, whereas other rock types are related to continental crust. The Pohorje nappe is folded into an ESE–WNW-striking antiform containing the Pohorje tonalite–granodiorite in its core (Figure 1b). The corresponding magma was mainly formed in continental crust (Altherr et al., 1995) and emplaced during the Early Miocene (Fodor et al., 2008:18.6 Ma U–Pb zircon; Trajanova et al., 2008:18–19 Ma K–Ar ages with a 16.7 Ma mean cooling age). The Pohorje nappe is overlain by Palaeozoic slate and phyllite. The upper nappe or unit on top of these rocks consists of Permo-Triassic sandstone and conglomerate (Hauzenberger et al., 2016). Middle and upper units should represent the Upper Central Austroalpine (Janák et al., 2006) in the Pohorje Mts.

The timing of metamorphism in the Pohorje nappe is generally accepted to be Eo-Alpine (Sandmann et al., 2016). The

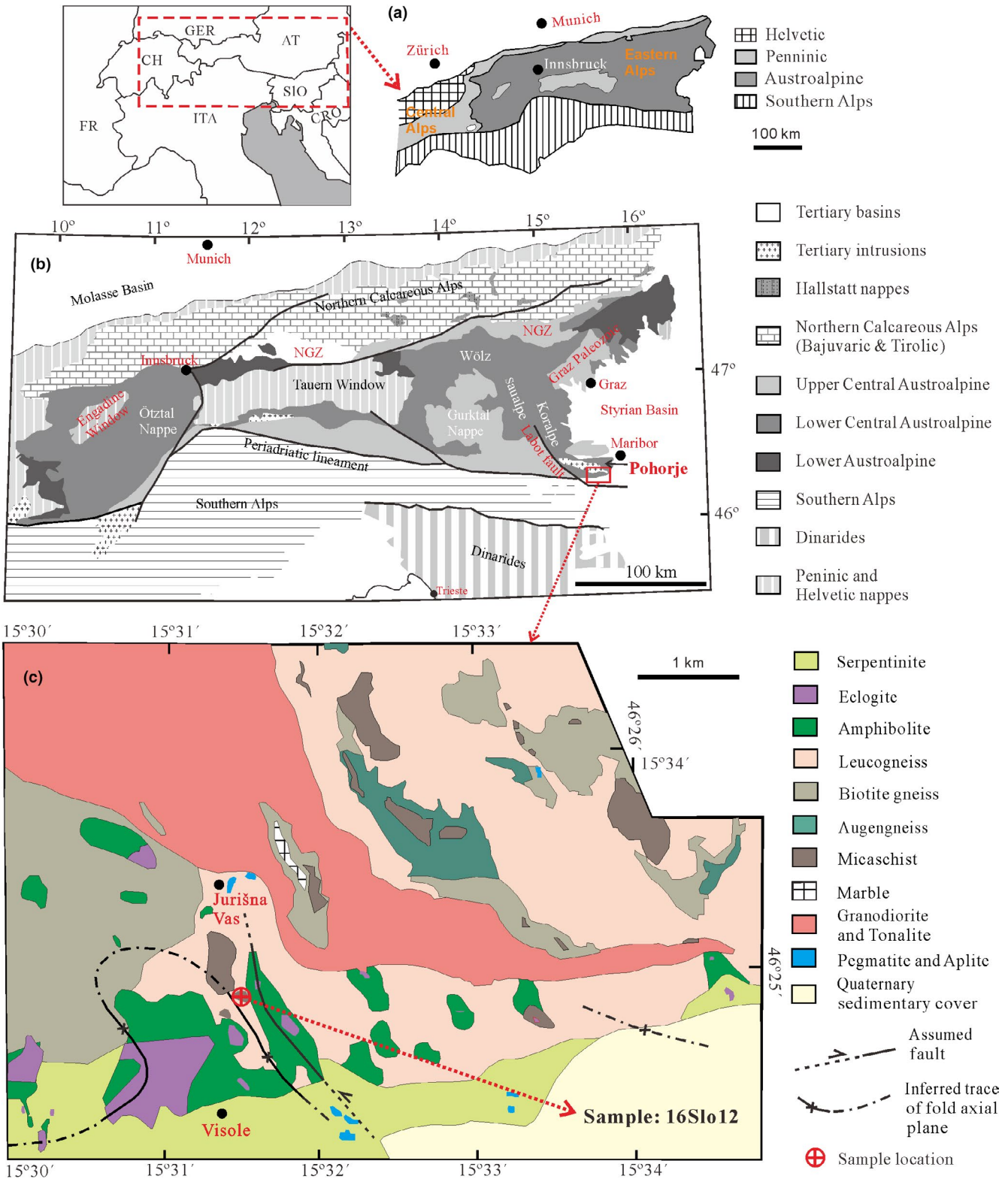

FIGURE 1 (a) Tectonic map according to Ratschbacher et al. (1989) showing the main units of the Central and Eastern Alps with (b) a more detailed map after Uher et al. (2014) and Sandmann et al. (2016). (c) Geological map of the southeastern Pohorje (with sample location) after Kirst et al. (2010) and Uher et al. (2014)

precise metamorphic ages have been summarized in recent literature (De Hoog et al., 2009; Hauzenberger et al., 2016; Janák et al., 2006, 2015; Sandmann et al., 2016): U–Pb zircon ages of eclogite and metapelite are *c*. 93–90 Ma (Janák et al., 2009; Miller et al., 2005). These ages fit with Sm–Nd garnet ages of eclogite (Miller et al., 2005), gneiss

TABLE 1 The bulk-rock composition (wt%) of the studied micaschist was determined with an X-ray fluorescence (XRF) spectrometer. XRFA is the bulk-rock composition after subtracting 2.5 wt% FeO from the original composition. XRFB is the bulk-rock composition after adding previously leached SiO_2, Al_2O_3, CaO, MgO and MnO (see text) to the original bulk-rock composition. As explained in the text, XRF1 and XRF2 were modified from XRF and XRFA1 (XRFB1) from XRFA (XRFB). AEBC and BEBC are effective bulk-rock compositions after subtracting porphyroblastic garnet (Grt_{0-1}) and the early generation of potassic white mica (Ph_1)

Name	XRF			Used for PERPLE_X calculations					
	XRF	XRFA	XRFB	XRF1	XRF2	XRFA1	AEBC	XRFB1	BEBC
Comment		XRF minus 2.5 wt. FeO	XRF plus loss due to weathering	XRF normalized	XRF normalized	XRFA normalized	XRFA normalized minus Grt_{0-1}+Ph_1	XRFB normalized	XRFB normalized minus Grt_{0-1}+Ph_1
SiO_2	55.14	55.14	56.52	55.93	57.99	57.43	61.98	56.04	59.79
Al_2O_3	22.96	22.96	23.20	23.29	24.15	23.92	20.62	23.00	19.59
MnO	0.08	0.08	0.14	0.08	0.09	0.09	0.08	0.14	0.15
MgO	1.40	1.40	1.61	1.42	1.47	1.46	1.42	1.60	1.62
CaO	0.20	0.20	0.41	0.15	0.15	0.21	0.11	0.41	0.39
Na_2O	0.18	0.18	0.18	0.18	0.19	0.19	0.01	0.18	0.01
K_2O	4.63	4.63	4.63	4.69	4.87	4.82	3.13	4.59	2.92
TiO_2	1.05	1.05	1.05	1.06	1.10	1.09	1.28	1.04	1.19
P_2O_5	0.13	0.13	0.13	0.00	0.00	0.00	0.00	0.00	0.00
FeO	8.07	5.57	8.07	8.19	8.49	5.80	6.38	8.00	9.34
H_2O	5.51	N.C.	N.C.	5.00	1.50	5.00	5.00	5.00	5.00
SUM	99.34	N.C.	N.C.	100.00	100.00	100.00	100.00	100.00	100.00
Figure showing the corresponding pseudosection and garnet isopleths				Figure S1a, b	Figure S1c, d	Figure 10, S3	Figure 11, S5	Figure S2	Figure S4

Abbreviation: N.C., not considered.

and micaschist (Thöni, 2003), one Lu–Hf garnet age of eclogite (Thöni et al., 2008), and U–Th–Pb monazite ages of metapelite (Krenn et al., 2009). Furthermore, ages of *c*. 93–90 Ma are similar to those related to the eclogite facies metamorphism in the Koralpe–Saualpe terrane (Miller & Thöni, 1997; Thöni, 2003; Thöni & Jagoutz, 1992; Thöni & Miller, 1996, 2009). This age relation suggests that this terrane (see Figure 1b) and the Pohorje Mts. are part of the same subducted crust (Janák et al., 2004, 2009). U–Th–Pb monazite ages of *c*. 76 ± 16 Ma determined on metapelite were related to a decompression event by Krenn et al. (2009). K–Ar mica ages (13–19 Ma; Fodor et al., 2002) as well as apatite fission-track ages (10 Ma) determined on metamorphic rocks in the Pohorje Mts. (Sachsenhofer et al., 1998) indicate that the final exhumation occurred in the Early to Middle Miocene. Permian (*c*. 286 and 258 Ma)–Triassic (*c*. 238 Ma) ages from U–Pb zircon cores in metapelites were recognized and interpreted to reflect continental rifting (Janák et al., 2009).

Based on the reported UHP rocks in the Pohorje nappe a geodynamic scenario was proposed that included the closure of the Meliata Ocean in the north by a continent–continent or arc–continent collision, which was followed by intracontinental subduction of the Pohorje nappe and, thus, the Lower Central Austroalpine towards the southeast under the Upper Central Austroalpine in the Late Cretaceous (Janák et al., 2004, 2006, 2009, 2015; Kirst et al., 2010; Sandmann et al., 2016). Subsequently, exhumation of the UHP rocks should have occurred by slab extraction, a process in which, however, the entire HP–UHP rocks of the Pohorje and Koralpe–Saualpe terrane were involved (Herg & Stüwe, 2018). Stüwe and Schuster (2010) demonstrated that an intracontinental subduction zone in the Austroalpine nappes is mechanically plausible. Schorn and Stüwe (2016) presented the so-called Plankogel detachment as evidence for the intracontinental subduction model. This detachment in the Saualpe–Koralpe terrane is an east–west trending, south-dipping low-angle structure. The Eclogite Unit in the footwall of the detachment experienced peak *P–T* conditions of 23–24 kbar and 640–690°C in contrast to the amphibolite facies metapelites (12–14 kbar, 550–580°C) in the hangingwall (Schorn & Stüwe, 2016). The pressure difference between footwall and hangingwall meets the basic hypothesis of the initially proposed intracontinental subduction scenario with slab extraction (Froitzheim et al., 2003).

3 | ANALYTICAL METHODS

Bulk-rock compositions for pseudosection modelling were obtained with a PHILIPS PW2400 X-ray fluorescence (XRF) spectrometer. The analytical procedure is described by Massonne et al. (2018). Rock powder of the sample was analysed for water content with a LECO® RC-412 analyser. The analytical results are given in Table 1.

Chemical compositions of minerals were obtained by using a CAMECA SX100 electron microprobe (EMP) with five wavelength-dispersive spectrometers. Contents of Na, K, Mg, Ca, Fe, Al, Si, Mn, Ti and Cr (only garnet) or Ba in silicates, using a focused beam, and Fe-hydroxide rich areas (defocused beam of 10 μm) were quantitatively determined with 15 kV acceleration voltage and 10 or 15 (only garnet) nA beam current. For all analyses (except rutile and monazite) 20 s counting time per element on peak and background each were applied (for analytical errors see Massonne, 2012). Mineral formulae and molar fractions of components in silicates were calculated from EMP analyses with the program CALCMIN (Brandelik, 2009).

For Zr-in-rutile thermometry, the contents of Nb, Si, Fe, Zr and Cr (Ti was calculated) in rutile were obtained with a beam current and acceleration voltage of 150 nA and 15 kV respectively. The counting time for the Zr Lα-radiation, using natural zircon as standard, at the peak and the background was 360 s each. According to counting statistics, the analytical 1σ-error was ±15 ppm for Zr. A SiO_2 content above 0.3 wt% led to the exclusion of the corresponding analysis as it was probably influenced by nearby silicates (Zack et al., 2004). In case of an iron content above 1 wt% (calculated as Fe_2O_3), the analysis was abandoned as well, because ilmenite, a replacement product of rutile, could have disturbed the result.

The analytical procedure to determine the composition and age of monazite with the EMP was described by Massonne, Cruciani, et al. (2018). This procedure yields reasonable results for dating of Palaeozoic to Tertiary monazite (Li & Massonne, 2017, 2018; Lo Pò et al., 2016; Massonne, 2016; Massonne et al., 2018; Massonne, Cruciani, et al., 2018; Waizenhöfer & Massonne, 2017). A wide range of elements (Si, P, S, As, Ca, Y, La, Ce, Pr, Nd, Sm, Gd, Dy, Er, Pb, Th and U) was analysed in situ on thin sections which were hand-polished with polycrystalline diamond (size ~1 μm). An acceleration voltage of 20 kV and a beam current of 130 nA were employed. The one-sigma uncertainty was calculated by propagation of the 1σ errors of the counting rates of the peak and background intensities of the relevant elements. The detection limit (3σ) for Pb related to the single analysis is somewhat above 60 ppm. As monazite compositions in the studied sample contain 2.1–10.0 wt% ThO_2, a one-sigma error between 11.4 and 3.0 Ma resulted for the single analysis. The age and corresponding error of all monazite analyses were calculated with the Mincalc program (Bernhardt, 2007). The ISOPLOT program by Ludwig (2003) was used to obtain probability plots as well as mean ages and errors of monazite populations.

Back-scattered electron (BSE) images were taken with the EMP to document specific textural features. Also with

the EMP, X-ray maps for potassic white mica (Mg, Fe, Ti, Na, Ba) were produced with 15 kV acceleration voltage and 30 nA beam current. The elements Mn, Ca, Mg, Fe and Y were considered for the simultaneous production of X-ray maps of garnet using 15 kV acceleration voltage and 60 nA beam current. Other parameters for the X-ray mapping were 1–8 μm step width and 70–100 ms per step for garnet and 3 μm step width and 100 ms per step for white mica.

4 | PETROGRAPHY AND MINERAL CHEMISTRY

We collected several micaschist samples at exposures in rural roads and cuts by rural and forest roads at and south of the village of Jurišna Vas (Figure 1c). In this area, which was noted as Eo-Alpine HP belt in a map published by Thöni (2006), the so-called UHP micaschists should occur (see the simplified geological map in Janák et al., 2015). All sampled micaschists from this area are characterized by a platy aspect (one main foliation), a dulled silvery-shining surface due to high contents of white mica, and several modal percent of mm-sized garnet. Thin sections of these samples show that all garnet grains were partially replaced by zoned white to red-brownish very fine-grained masses (rich in Fe-hydroxide, see also below) which are considered as being mainly due to weathering rather than retrograde metamorphism. Micaschist samples 16Slo12 and 16Slo15 were selected for a detailed investigation because they show the least late alteration in the thin sections of the collected micaschists which contain the same main mineral assemblage with moderately different modal proportions and grain sizes. 16Slo12 was sampled at the cut of a rural road (coordinates: N46°24.905′, E15°31.468′, Figure 1c) almost 1 km south of Jurišna Vas. 16Slo15 was collected ~200 m southwest of 16Slo12 at the cut of a forest road (coordinates: N46°24.789′, E15°31.454′). The X-ray maps and EMP spot analyses indicate that garnet and white mica in 16Slo12 and 16Slo15 show similar compositions, zoning patterns and textural relationships. Thus, we decided to present subsequently only the results on sample 16Slo12 in detail.

The petrography of 16Slo12 is documented in Figures 2 and 3 by photomicrographs and BSE images. Figure 4 shows a sketch of the textural relationships of the minerals including their various generations. Chemical zoning of garnet and phengite is discernable in the X-ray maps of Figures 5 and 6. Representative EMP analyses of minerals, except rutile and monazite, are presented in Tables 2 (garnet) and 3 (other minerals). Mineral abbreviations used in the text, figures and tables are broadly those given by Whitney and Evans (2010) but also explained in figure legends. In addition, O-H-I was taken as abbreviation for the undefined iron hydroxide-rich mass that replaced garnet.

The micaschist is fine-grained and clearly foliated, with alternating quartz and potassic white mica layers (Figures 2a,b and 4). It contains potassic white mica (47–50 vol.%), quartz (21–22 vol.%), biotite (9 vol.%), garnet (7 vol.%), which is rimmed by O-H-I (4–6 vol.%) mainly as a weathering product, chlorite (6 vol.%), and kyanite (1.5 vol.%). Accessories are graphite, rutile, anatase (confirmed by Raman microspectroscopy), ilmenite, staurolite, albite, iron sulfide, apatite, monazite and zircon. The modal proportions of minerals (vol.%) were estimated from thin sections by point counting using a polarized light microscope.

Two distinct groups of garnet grains were observed. One group is porphyroblastic ($Grt_{0\text{-}1}$, ~1.5 mm in diameter), elongated along the main foliation, and broken (Figure 4). O-H-I occurs mainly in the formed cracks and along rims of garnet (Figure 3a,b). Especially on the basis of Mn maps (Figure 5), porphyroblastic garnet can be subdivided into two types, which are slightly zoned ($Grt_{0\text{-}1}$) or unzoned (Grt_1). The entire Grt_1 has the rim composition of $Grt_{0\text{-}1}$ with the following averaged molar fractions X of garnet components: 0.637 almandine, 0.243 pyrope, 0.108 grossular (+andradite), and 0.012 spessartine = $Alm_{0.637}Prp_{0.243}Grs_{0.108}Sps_{0.012}$. The averaged core composition of $Grt_{0\text{-}1}$ is $Alm_{0.623}Prp_{0.23}Grs_{0.122}Sps_{0.025}$. Thus, according to elemental profiles, there are only slight compositional changes from core to rim in the group of porphyroblastic garnet. The other group (~50% of the total garnet) consists of small grains (Grt_2: maximal 0.3 mm in diameter), which are locally also rimmed by O-H-I (Figure 5c) and elongated along the main foliation, but not broken. Grt_2 shows a compositional core ($Alm_{0.728}Prp_{0.16}Grs_{0.09}Sps_{0.022}$)–rim ($Alm_{0.711}Prp_{0.14}Grs_{0.11}Sps_{0.039}$) relation (Figure 5).

No minerals are included in Grt_2, but the porphyroblastic garnet and its O-H-I rim are characterized by multiphase inclusions: (a) rutile+biotite (Bt_0)+staurolite+graphite+quartz+monazite+zircon+apatite+Fe-sulfide occur in the $Grt_{0\text{-}1}$ core (Figure 3a,c,d). Such inclusions show an internal foliation (Figure 3a) which forms an angle with the external foliation, indicating different tectono-metamorphic evolutions. (b) $Grt_{0\text{-}1}$ rim and Grt_1 show similar inclusions as the $Grt_{0\text{-}1}$ core, except that staurolite is not present but kyanite instead (Figure 3e). (c) Inclusions of Bt_0+staurolite+rutile+kyanite+quartz, that were probably originally in a border domain of garnet core and rim, were found in O-H-I that had replaced garnet (Figure 3f,g). A late-stage kaolinite has formed in cracks in garnet together with chlorite (Figure 3h). These minerals also occur in O-H-I, the average composition of which (Table 3), including tiny enclosed kaolinite, chlorite, and probably other phyllosilicate flakes, is characterized by a high iron content (average 38.7 wt% as FeO). However, contents of some elements can be variable according to numerous defocused EMP analyses (SiO_2 = 4.5–43.8 wt%, Al_2O_3 = 12.2–35.0 wt%, MgO = 0–3.7 wt%, K_2O = 0–1.6 wt%, CaO = 0–0.25 wt%,

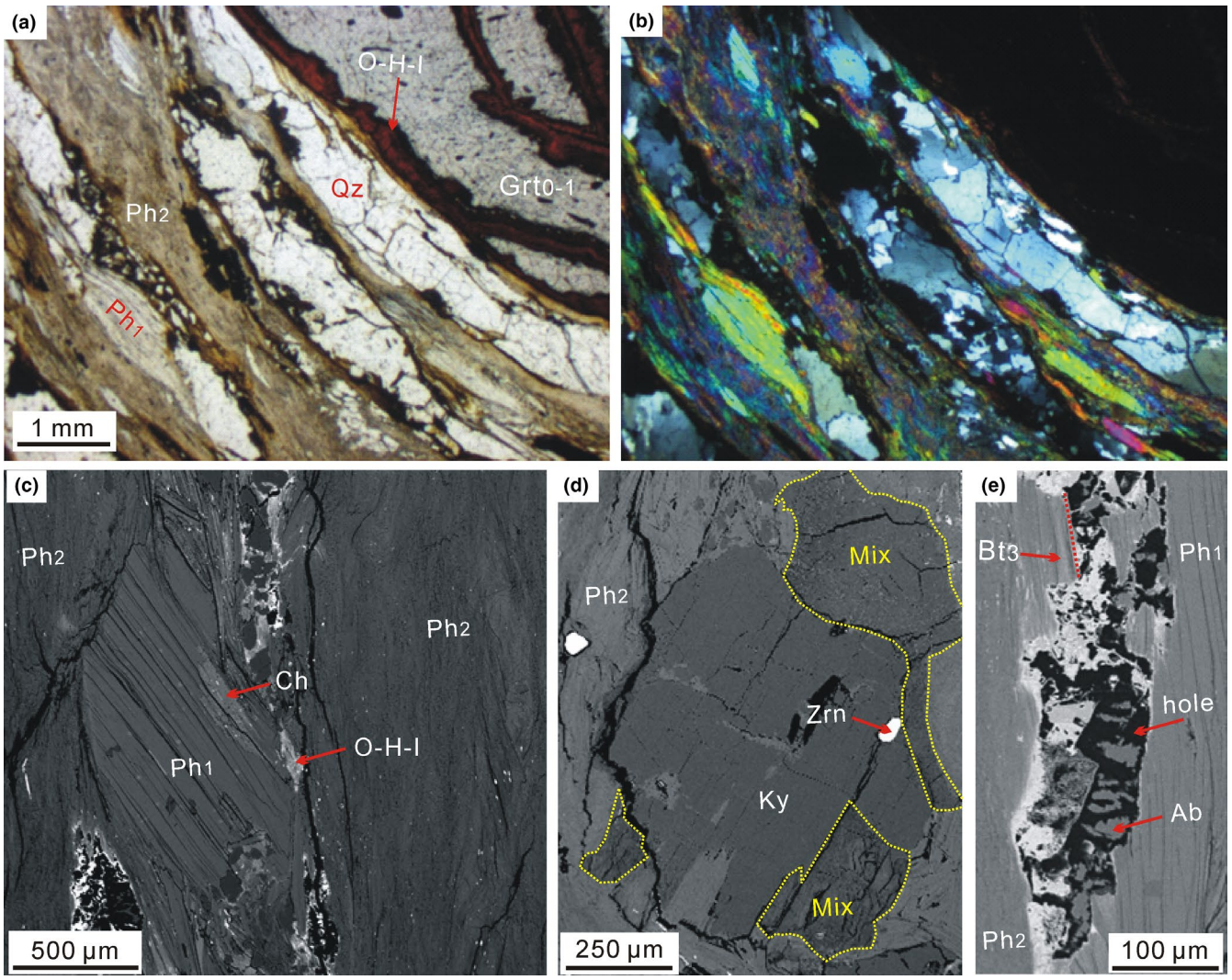

FIGURE 2 Photomicrographs taken on a thin section of metapelite 16Slo12 under plane polarized light (a) and crossed polarizers (b). Back-scattered electron images (c–e) show textural features. (a, b) Alternating quartz and potassic white mica layers. Garnet is rimmed by an undefined iron hydroxide-rich mass (O-H-I). (c) Coarse-grained (Ph_1) and fine-grained white mica (Ph_2). (d) Kyanite (Ky) and its replacement product (Mix) being a mixture of mainly potassic white mica, quartz and probably other unidentifiable phases. (e) Relictic albite elongated along the main foliation and broken. Late, retrograde biotite (Bt_3) and Ph_2 are part of this elongated aggregate. For mineral abbreviations see text

Na_2O = 0–0.14 wt%; MnO = 0–0.10 wt%; sum of oxides = 73.9–84.0 wt%).

White mica forms two main generations with almost identical modal abundances. The younger generation (Ph_2) typically grew as mica aggregates (average single grain size ~ 0.15 × 0.06 mm^2) along the main foliation (Figure 2a–c). The older generation (Ph_1) is characterized by millimetre-sized, thick flakes (Figures 2a–c and 4), which are the relics of former coarser grains. Ph_1 was probably forced to align along the main foliation and is surrounded by Ph_2. All white mica is potassic with a strongly variable composition. Ph_1 shows significantly higher Na contents of 0.06–0.15 per formula unit (pfu; Si = 3.04–3.22 pfu) than Ph_2 (Na = 0.01–0.03 pfu; Si = 3.04–3.27 pfu; Figure 6). Very fine-grained potassic white mica (Ph_3) is part of diverse replacement products, for instance, around kyanite (Figure 2d) and garnet.

Small biotite flakes (Bt_3), aligned along the main foliation together with Ph_2, are richer in Ti (Ti = 0.10–0.12 pfu; Fe/(Fe+Mg)=*X*Fe = 0.25–0.37) than biotite (Bt_0: Ti = 0.06–0.08 pfu; *X*Fe = 0.24–0.41 pfu) included in various garnet domains. Chlorite with *X*Mg=Mg/(Mg+Fe+Mn) of 0.35–0.41 occurs only in the matrix around garnet, as possible replacement product of white mica or in fractures of garnet.

Matrix albite (grain size < 0.05 × 0.05 mm^2) is elongated along the main foliation and broken with *X*Na=Na/(Na+K+Ca) of 0.98–1.0 (Figure 2e). Apatite occurs in garnet and in the matrix. Rutile is the TiO_2 phase that was only found as inclusion in garnet whereas anatase appears in the matrix. Ilmenite is a local replacement product of anatase. Staurolite, enclosed in porphyroblastic garnet (Grt_{0-1} and Grt_1) and O-H-I, contains constant Mg contents with $Mg/(Mg+Fe^{2+}+Zn+Mn)$ = 0.28. However, staurolite in

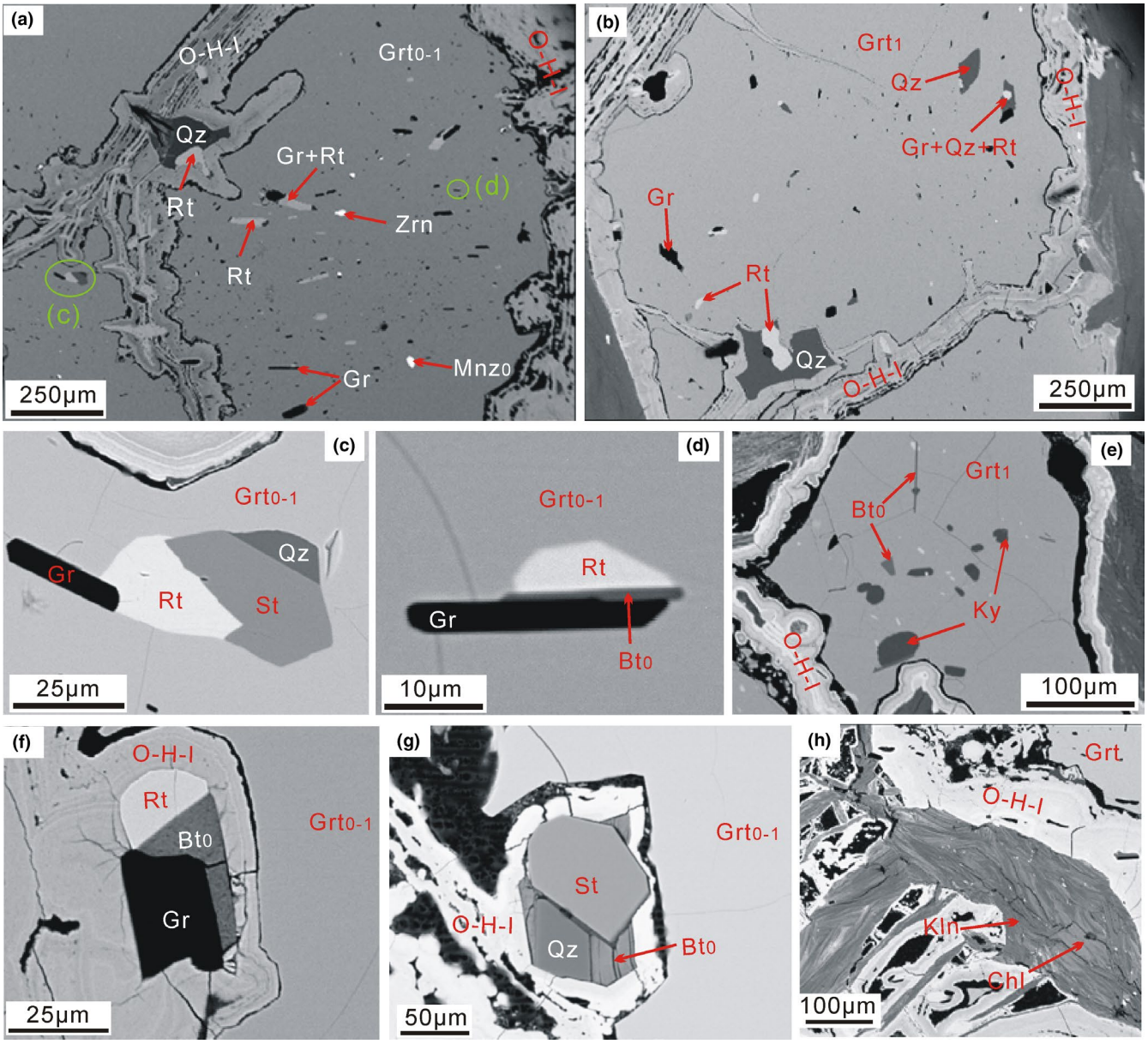

FIGURE 3 Back-scattered electron images of objects in metapelite 16Slo12. (a, b) Garnet is rimmed by an undefined iron hydroxide-rich mass (O-H-I) which also fills cracks in garnet. (c–e) Mineral inclusions in porphyroblastic garnet. (f, g) Inclusions in the former rim of garnet that is replaced by O-H-I. (h) Kaolinite and chlorite as late retrograde products in cracks of garnet accompanied by O-H-I. For mineral abbreviations see text

porphyroblastic garnet shows slightly higher ZnO (~5.0 wt%) and TiO_2 (0.95 wt%) contents than staurolite (ZnO = 3.4 wt%, TiO_2 = 0.6 wt%) in O-H-I, that is, in the replaced garnet core-rim border domain (see above).

5 | MONAZITE TEXTURE, CHEMICAL COMPOSITION AND U–Th–Pb DATING

Ninety-three EMP analyses were achieved on monazite in sample 16Slo12. Since high Th/U ratios in monazite generally result from fluid-related alterations (Hoisch et al., 2008; Janots et al., 2012; Seydoux-Guillaume et al., 2012; Williams et al., 2011), we ignored four analyses (Th/U mass ratio = 19–43) for further dating considerations (thus, 89 monazite analyses are plotted in Figure 7b, c). Representative monazite analyses are given in Table 4. The petrographic context, chemical data and obtained ages are summarized in Figures 7–9.

Monazite occurs in three different microstructural settings: (a) Inclusions of subhedral grains (Mnz_0: 20–30 μm in diameter) occur in porphyroblastic garnet (Grt_{0-1} and Grt_1: four analyses on two monazite grains; Figure 8a). Zoning in these monazite grains was not observed in BSE images. The obtained ages are between 285.8 ± 6.5 Ma and 301.1 ± 7.6

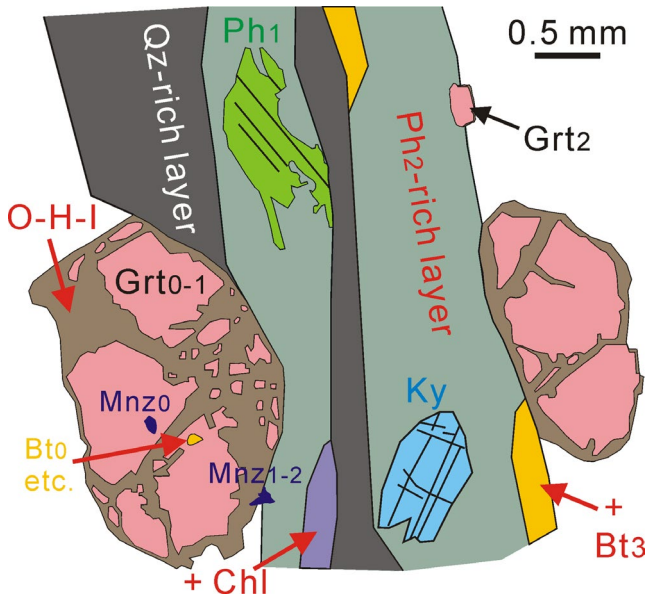

FIGURE 4 Sketch of the texture of the studied micaschist 16Slo12. For mineral abbreviations see text. The sequence of minerals is partially marked with subscripts 0 (refering to the oldest minerals, included in garnet, eventually coexisting with an undetectable garnet = Grt_0) to 3 (the latest minerals formed during late retrogression and weathering). The areas coloured dark yellow and light purple in Ph_2-rich layers are related to the dominance of late biotite and chlorite in these layers. Further information on the texture is given in the text

(1σ) Ma. (b) Inclusions were also found in the former garnet rim now replaced by O-H-I (14 analyses on 5 monazite grains; Figure 8b). These monazite grains ($Mnz_{0\text{-}1}$:10–50 μm in diameter) show anhedral shape with irregular edges and irregular zoning in all grains. The obtained ages can be related to two clusters between 271.0 ± 3.6 and 306.7 ± 9.5 (1σ) Ma and between 86.2 ± 6.5 and 108.4 ± 6.9 (1σ) Ma. Monazite of both age groups shows dark and light BSE domains. (c) In the matrix (71 analyses on 23 monazite grains = Mnz_2; Figure 8c) monazite grains form clusters (reaction products of former allanite?—see Massonne, 2016; Spear, 2010) which were mainly found in potassic white mica. These grains are commonly euhedral, elongated and broken being 10–30 μm in diameter (Figure 8c). BSE images show complex zonation patterns discernable by bright domains, which could be in the inner part or along fractures of a grain. The bright domains are frequently slightly younger than the dark domains, but all ages of matrix monazite are between 14.0 ± 5.6 and 63.0 ± 7.9 (1σ) Ma except for one large monazite relic (100 × 300 μm^2) with no visible zonation enclosed in quartz (Figure 8c). The eight ages obtained on this relic range between 86.3 ± 5.8 and 103.9 ± 5.9 (1σ) Ma.

Altogether four age populations were recognized by histogram analysis with ISOPLOT (Figure 9a). These populations also show specific chemical compositions (Figure 7). The oldest population (12 analyses with a weighted mean age of 283.6 ± 6.1 (2σ) Ma, MSWD = 2.4) (Figure 9b), referring to Mnz_0 included in porphyroblastic garnet and in O-H-I (Figure 8a,b), is characterized by relatively high Y contents (0.85–1.42 wt% Y, average 1.15 wt%, Figure 7b) and low La/Gd mass ratios (7.2–12.2, average 8.7, Figure 7c). A younger age population (14 analyses with a weighted mean age of 94.1 ± 3.7 (2σ) Ma, MSWD = 1.3, Figure 9c) is defined by monazite (Mnz_1) included in the garnet rim (replaced by O-H-I) and the monazite relic enclosed in quartz (Figure 8b,c). This population contains low Y contents of 0.03–0.20 wt% (average: 0.05 wt%) and high La/Gd ratios of 13.2–28.3 (average: 21.4; Figure 7b,c) and, thus, resembles the 10–50 μm-sized M_1 type of monazite in the studied area of the Pohorje Mts. dated by Krenn et al. (2009: 100 ± 6 Ma). The youngest monazite (Mnz_2, n = 63) with single ages from 14.0 ± 5.6 (1σ) Ma to 63.0 ± 7.9 (1σ) Ma is exclusively related to the monazite clusters in the matrix (Figure 8c). A subdivision into two populations results from the probability analysis with ISOPLOT (Figure 9d) leading to weighted mean ages of 47.9 ± 10.8 (2σ) Ma (Mnz_{2a}: single ages between 42.4 ± 8.3 and 63.0 ± 7.9 (1σ) Ma, MSWD = 1.01) and 26.2 ± 2.8 (2σ) Ma (Mnz_{2b}: between 14.0 ± 5.6 and 36.4 ± 3.8 Ma, MSWD = 1.04). Mnz_{2a} has high Y contents (1.0–1.5 wt%, average: 1.1 wt%) and low La/Gd ratios (6.2–11.2, average: 10.6) (Figure 7b,c). The younger Tertiary population is characterized by a spread of both Y contents (0.03–1.4 wt%, average: 0.5 wt%) and La/Gd ratios (6.1–32.1, average: 19.9; Figure 7b,c).

6 | *P–T* EVOLUTION

6.1 | Calculation method for *P–T* pseudosections

P–T pseudosections were calculated with PERPLE_X (see Connolly, 2005), an internally consistent thermodynamic data set for minerals (Holland & Powell, 1998, or Holland & Powell, 2011), and the model CORK (Holland & Powell, 1991) for H_2O for the *P–T* range 3–25 kbar and 450–700°C. Different thermodynamic data sets and effective bulk-rock compositions (EBCs) were used for reasons explained below. Selected *P–T* pseudosections were worked out in detail by contouring them with isopleths of various parameters, which were mainly those related to the chemical composition of garnet. As suggested by Connolly (2005) the raw curves obtained with PERPLE_X were smoothed.

6.1.1 | Thermodynamic data used

One set of thermodynamic data used (here called: thermodynamic data set 1) refers to those downloaded in August

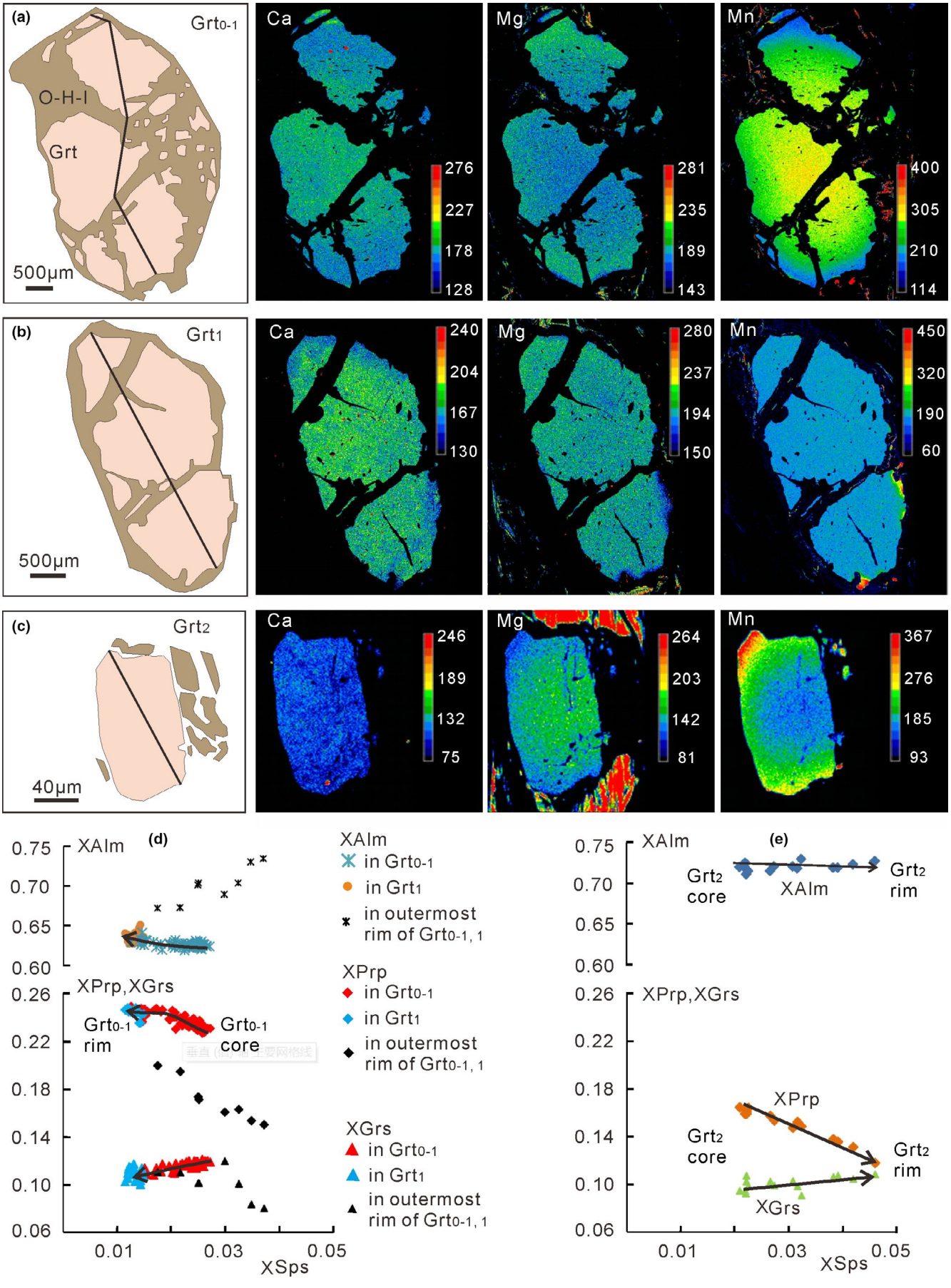
(a)
Grt0-1
O-H-I
Grt
500μm
Ca
276
227
178
128
Mg
281
235
189
143
Mn
400
305
210
114
(b)
Grt1
500μm
Ca
240
204
167
130
Mg
280
237
194
150
Mn
450
320
190
60
(c)
Grt2
40μm
Ca
246
189
132
75
Mg
264
203
142
81
Mn
367
276
185
93
(d)
XAlm
0.75
0.70
0.65
0.60
XPrp,XGrs
0.26
0.22
0.18
0.14
0.10
0.06
Grt0-1 rim
Grt0-1 core
0.01
0.03
0.05
XSps
XAlm
in Grt0-1
in Grt1
in outermost rim of Grt0-1, 1
XPrp
in Grt0-1
in Grt1
in outermost rim of Grt0-1, 1
XGrs
in Grt0-1
in Grt1
in outermost rim of Grt0-1, 1
(e)
XAlm
Grt2 core
Grt2 rim
XPrp,XGrs
XPrp
XGrs
Grt2 core
Grt2 rim
XSps

FIGURE 5 (a–c) X-ray maps of garnet (sample 16Slo12) showing the distribution of Ca, Mg and Mn in porphyroblastic garnet (a, b) and late small garnet (Grt_2). The colour scales on the right hand side each refer to counts of specific Kα-radiation per time unit. (d) Compositional profiles across the garnet grains exhibited in (a–c) show variations in the molar fractions XPrp, XGrs, XSps and XAlm. For mineral abbreviations see text

2011 from the PERPLE_X web-site. The applied thermodynamic solid-solution models for this version (see file solution_model1.dat in Massonne, Cruciani, et al., 2018) are the following: (a) Carp(M) for carpholite (Massonne & Willner, 2008); (b) Chl(HP) for chlorite (Holland et al., 1998); (c) Ctd(HP) for chloritoid (White et al., 2000); (d) feldspar for plagioclase and K-feldspar (Fuhrman & Lindsley, 1988); (e) Gt(HP) for garnet (Holland & Powell, 1998); (f) hCrd and IlGkPy (maximum 30 mol.% geikilite component) are ideal solutions used for cordierite and ilmenite, respectively, based on the thermodynamic data for corresponding end-members given by Holland and Powell (1998); (g) GlTrTsPg for amphibole (e.g. Wei et al., 2003), which is not inferior to more recently created amphibole models (Li et al., 2017); (h) Mica(M) for paragonite with maximal 50% muscovite component (Massonne, 2010); (i) Omph(HP) for clinopyroxene (Holland & Powell, 1996; Zeh et al., 2005); (j) Opx(HP) for orthopyroxene (Powell & Holland, 1999); (k) Pheng(HP) for phengite (Holland & Powell, 1998) with maximal 50% paragonite component; (l) TiBio(HP) for biotite (Powell & Holland, 1999; White et al., 2000); (m) St(HP) for staurolite, and T for talc were taken 'from THERMOCALC' (written comm. by J.A.D. Connolly). Quartz, zoisite, rutile, Al-silicates and lawsonite were considered as pure phases. We excluded mica (tip, tbi, ann1), feldspar (mic), amphibole (rieb, mrb, cumm, grun) and melt (h2oL) components and the O_2 buffers qfm and mthm. For instance, these mica components were neglected because of their untrustworthiness (Massonne, Cruciani, et al., 2018).

A more recent set of thermodynamic data (here called: thermodynamic data set 2), downloaded in December 2018 from the PERPLE_X web-site including an updated version (6.8.0) of the PERPLE_X software package, was used for comparison. Significant differences between the results obtained from both data sets applied here could point to a possible revision of older *P–T* results published in the literature. In addition to the data set of Holland and Powell (2011), enhanced solid-solution models were used: (a) Chl(W) and Ctd(W) for chlorite and chloritoid, respectively, by White et al. (2014), (b) Carp(SGH) for carpholite by Smye et al. (2010), (c) Gt(WPPH) for garnet (see file solution_model.dat in recent PERPLE_X updates) by White et al. (2007), (d) Amph(DHP) for amphibole by Dale et al. (2000), and (e) Bio(TCC) for biotite by Tajčmanová et al. (2009). The models Pheng(HP), Mica(M), Omph(HP), Opx(HP), St(HP), feldspar, hCrd, T and IlGkPy were applied again. We excluded feldspar (mic) and melt (h2oL) components and the O_2 buffers qfm and mthm.

6.1.2 | Effective bulk-rock compositions

The PERPLE_X calculations were undertaken in the model system Na_2O–K_2O–CaO–FeO–MnO–MgO–Al_2O_3–SiO_2–

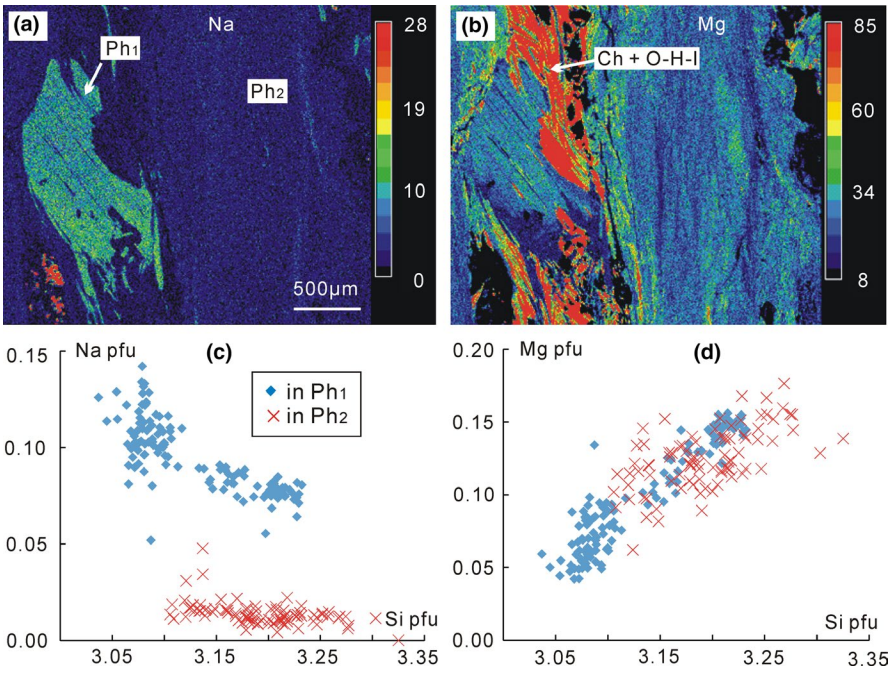

FIGURE 6 Na and Mg concentration maps (a, b) and analytical data obtained by EMP analyses of potassic white mica (c, d) in sample 16Slo12. The colour scales on the right-hand side each refer to counts of specific Kα-radiation per time unit. For mineral abbreviations see text

TABLE 2 Representative EMP analyses (wt%) of garnet in sample 16Slo12. Its structural formula (double unit) was calculated on the basis of 24 O and 10 six- and eightfold coordinated cations. Molar fractions of garnet components are given at the bottom. Abbreviations as given in the text

Comment	Grt_{0-1} core	Grt_{0-1} rim	Grt_2 core	Grt_2 rim
SiO_2	38.81	38.88	38.30	38.24
TiO_2	0.01	0.00	0.00	0.01
Al_2O_3	22.17	22.32	21.67	21.66
Cr_2O_3	0.01	0.01	0.00	0.01
Fe_2O_3	0.00	0.00	0.00	0.00
FeO	28.99	30.38	32.47	32.41
MnO	1.16	0.52	0.98	1.74
MgO	6.17	5.79	4.07	3.42
CaO	4.24	3.59	3.20	3.76
Na_2O	0.00	0.00	0.00	0.01
Total	101.56	101.49	100.68	101.25
Si	5.963	6.015	6.078	6.045
Ti	0.001	0.000	0.000	0.001
Al	4.013	4.069	4.052	4.035
Cr	0.001	0.002	0.000	0.001
Fe^{3+}	0.000	0.000	0.000	0.000
Fe^{2+}	3.724	3.930	4.309	4.285
Mg	1.412	1.335	0.963	0.806
Ca	0.699	0.595	0.544	0.637
Mn	0.151	0.068	0.131	0.234
Na	0.000	0.000	0.000	0.002
Sps	0.025	0.012	0.022	0.039
Grs	0.117	0.100	0.092	0.107
Prp	0.236	0.225	0.162	0.135
Alm	0.622	0.663	0.725	0.719

TiO_2–H_2O. Fe_2O_3 was ignored because of the presence of graphite in garnet and matrix suggesting a low oxygen fugacity. In addition, equilibrium phase relations are only slightly influenced by some trivalent iron as was demonstrated for pelites of medium metamorphic grade by Massonne (2014), Massonne, Cruciani, et al. (2018), Rahimi and Massonne (2018), and Waizenhöfer and Massonne (2017).

The bulk–rock composition determined with XRF (Table 1) was modified considering the subsequent procedures. (a) The H_2O content was set to 5 wt% to permit the formation of a free hydrous fluid phase at relatively low temperatures. (b) The analysed P_2O_5 content was set to zero. Massonne (2012) and Massonne and Toulkeridis (2012) suggested to reduce the CaO content of apatite-bearing rocks, according to the P_2O_5 content in the bulk rock. However, no Ca was subtracted here as monazite is present in the rock and apatite is very rare. The consequence of this decision and the low CaO content in sample 16Slo12 (Table 1) is a relatively high uncertainty of the *P–T* position of the isopleths for the grossular content in garnet (Massonne, Cruciani, et al., 2018). The results of the above procedures to modify the original bulk-rock composition are given in Table 1 after normalization to 100% each.

Due to the partial replacement mainly of garnet by alteration (very late retrogression+weathering) products (O-H-I, see above), we had to consider a change of the original bulk-rock composition. Two different strategies were used to reconstruct this composition: (a) According to the above description of O-H-I (average composition in Table 3) Fe is enriched in this mineral mixture compared to the composition of the enveloped garnet. We subtracted 2, 2.5 or 3.0 wt% of FeO from the XRF composition to account for this Fe enrichment by weathering that had led to roughly 5 vol.% of O-H-I in the rock. The results of test calculations with PERPLE_X are similar for the three bulk-rock compositions obtained after subtraction of FeO. Therefore, we present subsequently only the *P–T* pseudosection and isopleths for garnet components after subtraction of 2.5 wt% FeO (Table 1: XRFA). (b) Strategy A could result in a deficit of almandine-rich garnet in the original micaschist because we removed iron that was possibly before in garnet. Strategy B considers this possibility which implies that the Fe content was fixed in the rock. Instead other elements were leached from garnet by water during the weathering process. Solved Fe^{2+} could be in situ precipitated as insoluble Fe^{3+}-oxide/hydroxide by near-surface oxidation. The same might be true for Al in hydroxide and phyllosilicate (together with Si, e.g. as kaolinite). The loss of specific cations can be described by the bulk reaction: garnet+H_2O (+O_2)=O-H-I+escaped rest (nearly all Ca and Mg from the garnet). We estimated this loss and added it to the XRF composition to obtain the original micaschist composition (Table 1: XRFB). For this estimation (see Table S1), the difference of garnet composition (average of Grt_{0-1} rim and entire Grt_2) and the mean composition of O-H-I multiplied with a factor Z was considered. The result using $Z = 0.06$ (modal content of O-H-I = 0.05 multiplied by 1.2 because of considerable mass loss, but lower density and significant water content of O-H-I compared to garnet) yields the amount of oxides (1.38 wt% SiO_2, 0.24 wt% Al_2O_3, 0.06 wt% MnO, 0.21 wt% MgO, 0.21 wt% CaO) added to the XRF composition of Table 1 to obtain composition XRFB. The results of the above procedures to approach the original bulk-rock composition are given in Table 1 considering procedures 1 and 2 and normalization to 100% each.

Although no melting was noted to have occurred in micaschist sample 16Slo12, we calculated the solidus curve for the bulk-rock composition obtained by XRF. This curve is considered to be the upper temperature limit for the rock studied. The calculation was achieved for the XRF composition

TABLE 3 Representative EMP analyses (wt%) of minerals in sample 16Slo12. Structural formulae were calculated as follows: micas: O = 11; albite: O = 8; chlorite: O = 28; staurolite: number of cations = 30 (without H assumed to be 2). Mineral abbreviations as given in the text

	O-H-I	Bt_0	Bt_3	Ab	Chl	St	St	Ph_1	Ph_1	Ph_2	Ph_2
	Normalized mean	in Grt	in matrix	in matrix	in matrix	in Grt_1	in O-H-I	High Na	High Na	Low Na	Low Na
SiO_2	17.80	36.38	37.76	68.61	27.71	27.31	27.08	47.31	45.93	48.87	46.23
TiO_2	0.08	1.35	1.96	0.00	0.12	1.08	0.62	0.69	0.74	0.13	0.27
Al_2O_3	20.92	20.84	19.40	20.11	22.63	53.28	53.06	31.31	34.56	30.60	33.65
$(FeO)_{tot}$	38.69	14.59	10.42	0.24	29.27	8.92	10.51	1.51	0.95	2.78	1.36
MnO	0.04	0.09	0.02	0.04	0.15	0.05	0.02	b.d.l.	b.d.l.	0.07	0.00
MgO	0.70	12.07	16.08	b.d.l.	9.26	3.02	2.96	1.46	0.69	1.44	0.83
ZnO	N.D.	N.D.	N.D.	N.D.	N.D.	4.95	3.42	N.D.	N.D.	N.D.	N.D.
CaO	0.08	0.02	0.09	0.38	b.d.l.	N.D.	N.D.	0.02	b.d.l.	0.13	0.00
Na_2O	0.04	0.33	0.41	11.58	b.d.l.	N.D.	N.D.	0.60	0.76	0.06	0.36
K_2O	0.27	8.68	8.67	0.07	b.d.l.	N.D.	N.D.	10.38	10.13	10.69	10.09
BaO	0.01	0.09	0.10	0.00	b.d.l.	N.D.	N.D.	0.16	0.29	0.04	0.16
H_2O_{calc}	21.37	4.03	4.13	n.c.	11.48	1.07	1.06	4.41	4.43	4.47	4.42
Total	100.00	98.47	99.04	101.02	100.60	99.68	98.73	97.86	98.06	99.29	97.37
Si	n.c.	2.707	2.741	2.970	5.790	7.687	7.677	3.216	3.081	3.277	3.137
Ti	n.c.	0.076	0.107	0.000	0.013	0.230	0.132	0.035	0.038	0.006	0.014
Al	n.c.	1.828	1.659	1.026	5.573	17.677	17.728	2.509	2.759	2.419	2.691
Fe^{3+}	n.c.	n.c.	n.c.	0.009	n.c.	n.c.	n.c	n.c.	n.c.	n.c.	n.c.
Fe^{2+}	n.c.	0.908	0.633	n.c.	5.115	2.099	2.491	0.086	0.054	0.156	0.077
Mn	n.c.	0.006	0.001	0.001	0.026	0.013	0.005	0.000	0.000	0.004	0.000
Mg	n.c.	1.339	1.740	0.000	2.884	1.268	1.250	0.148	0.070	0.144	0.084
Zn	N.D.	N.D.	N.D.	N.D.	N.D.	1.028	0.716	N.D.	N.D.	N.D.	N.D.
Ca	n.c.	0.002	0.007	0.018	n.c.	N.D.	N.D.	0.002	0.000	0.009	0.000
Na	n.c.	0.048	0.058	0.972	n.c.	N.D.	N.D.	0.079	0.102	0.008	0.005
K	n.c.	0.824	0.803	0.004	n.c.	N.D.	N.D.	0.901	0.876	0.904	0.926
Ba	n.c.	0.003	0.003	0.000	n.c.	N.D.	N.D.	0.004	0.008	0.001	0.004
H	n.c.	2.000	2.000	n.c.	16.000	2.000	2.000	2.000	2.000	2.000	2.000

Abbreviations: b.d.l., below detection limit; n.c., not calculated; N.D., not determined.

with only 1.5 wt% H_2O added and application of procedure 2 (XRF2 in Table 1). For the corresponding PERPLE_X calculation we added the haplogranitic melt model melt(HP) by Holland and Powell (2001) and White et al. (2001).

In order to approach the EBC for a late metamorphic stage at which small garnet (Grt_2, see above) formed, we subtracted the chemical composition of the porphyroblastic garnet (Grt_{0-1}, Grt_1) and the early generation of potassic white mica (Ph_1, Figure 2a–c) from the bulk-rock composition (Table 1: XRFA and XRFB) according to the following principle (see Waizenhöfer & Massonne, 2017): the volume (corresponding to the area in a thin section) of porphyroblastic garnet (here: 4 vol.%) and of Ph_1 (here: 20 vol.%) with respect to the bulk rock (100 vol.%) was determined. The means of the chemical compositions of these mineral domains were calculated based on the obtained EMP analyses. The resulting compositions with the determined proportions (also considering the different densities of garnet, potassic white mica and bulk rock) were subtracted from the reconstructed compositions of the original bulk-rock composition of sample 16Slo12 (XRFA, XRFB). Subsequently, the obtained compositions were normalized to 100 wt% with 5 wt% H_2O (Table 1: AEBC, BEBC).

6.2 | Results of the calculated *P–T* pseudosections

Finally, eight calculated *P–T* pseudosections were worked out in detail for metapelite 16Slo12. Two *P–T* pseudosections (Figure S1) were obtained with thermodynamic data set 1 for the slightly modified XRF composition with 5 and 1.5 wt%

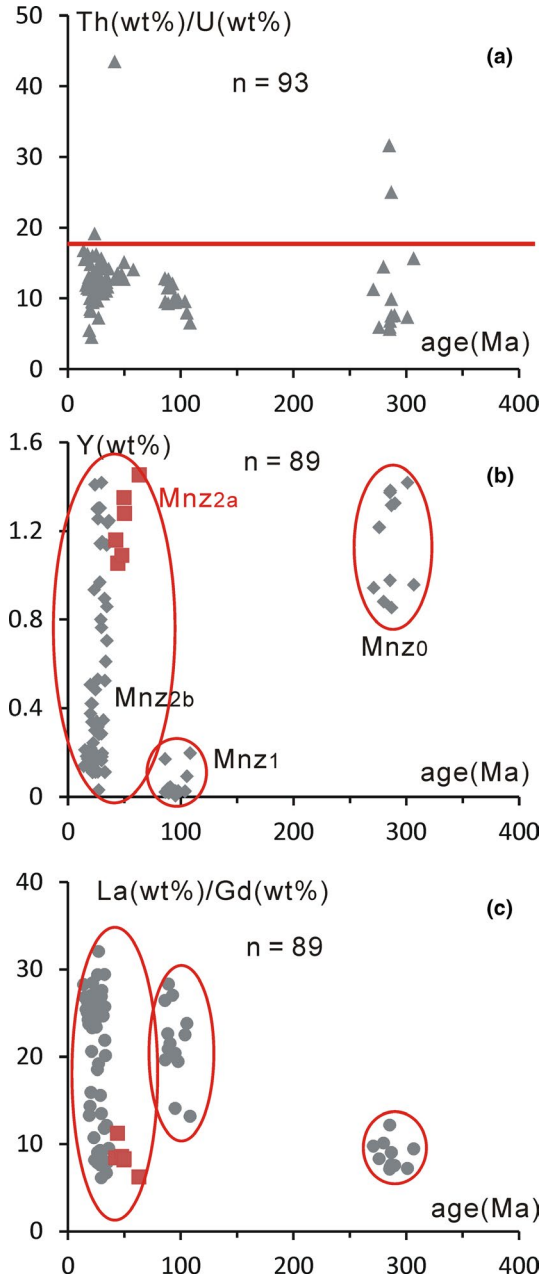

FIGURE 7 Graphical presentation of the chemical compositions of monazite analysed with the EMP: (a) Th/U mass ratio shown for all analyses. (b, c) Data for all analyses minus those four with high Th/U ratio (see a) concerning Y contents (b) and La/Gd mass ratios (c). Three age clusters are clearly discernable. The youngest one can be subdivided into an older population characterized by high Y contents (red boxes) and a younger population with high to low Y contents

H_2O (Table 1: XRF1, XRF2). The latter pseudosection was mainly used to determine the *P–T* position of the solidus, which is located at temperatures above 670°C at pressures above 5 kbar. Further two pseudosections (Figures 10a and 11a) were calculated with thermodynamic data set 1 for the XRF composition after subtracting 2.5 wt% of FeO (strategy A, Table 1: XRFA1) and the corresponding EBC (AEBC). Additional two *P–T* pseudosections (Figures S2a and S4a) were computed with this data set for the XRF composition after adding element quantities, assumed to be leached during alteration of garnet, (strategy B, Table 1: XRFB1) and the corresponding EBC (BEBC). Moreover, we used thermodynamic data set 2 to calculate two *P–T* pseudosections (Figures S3a and S5a) for the XRF composition after subtracting 2.5 wt% of FeO and the corresponding EBC (AEBC) again.

If we compare the three *P–T* pseudosections (Figure 10a and Figure S2a, one is not shown) calculated with thermodynamic data set 1 for modified XRF compositions with 5 wt% H_2O (Table 1: XRF1, XRFA1, XRFB1), the *P–T* locations of specific isopleths for Si pfu in potassic white mica are virtually identical. The relevant *X*Grs (0.10–0.12, Table 2) isopleths for $Grt_{0–1}$ in these pseudosections differ little at HP conditions (10–18 kbar). These isopleths are located close to 600°C. However, the relevant *X*Prp (~0.23) isopleths differ significantly. They are located either above 700°C at HP conditions for compositions XRF1 and XRFB1 or relatively close to the XGrs isopleths for composition XRFA1. The comparison of the two pseudosections (Figure 11a and Figure S4a), calculated for AEBC and BEBC (Table 1), yields a good coincidence of the relevant *X*Grs (~0.10, Table 2) and *X*Prp (~0.15) isopleths for the small garnet Grt_2.

Concerning the comparison of pseudosection calculations (Figure 10a and Figure S3a; Figure 11a and Figure S5a) with the different thermodynamic data sets 1 and 2 of Section 6.1.1, we figured out that the resulted *P–T* conditions for the formation of porphyroblastic (bulk-rock composition XRFA1) and small garnet (AEBC), based on the isopleths for Si pfu in potassic white mica and *X*Prp and *X*Grs in garnet, are almost identical. The most significant differences were that (a) the *P–T* positions of the isopleths for Grt_2 shift by 40°C at ~20 kbar from 575 to 620°C (thermodynamic data set 1) to 540–580°C (thermodynamic data set 2) and (b) the kyanite and staurolite fields are enlarged at pressure >16 and <16 kbar, respectively, using thermodynamic data set 2 instead of 1 (compare Figure 11a and Figure S5a).

Because of the close approach of relevant garnet isopleths (*X*Prp, *X*Grs) only in *P–T* pseudosections for XRFA and AEBC, we present details in the following exclusively for calculation results after applying strategy A. The subsequently given *P–T* ranges include errors as suggested, for instance, by Massonne (2013). In various *P–T* graphs we show circles confining *P–T* conditions related to the formation of relatively coarse-grained minerals (Ph_1, $Grt_{0–1}$) whereas error ellipses, as proposed by Li et al. (2017), are presented for the late metamorphic stage at which fine-grained minerals (Ph_2, Grt_2) formed. For the Si-in-potassic white mica barometry (Si isopleths for mica in pseudosections), which is not so pressure sensitive for Al-rich metapelites as for other rock types especially orthogneisses, we assume (2σ) errors of ±2 kbar.

TABLE 4 Representative EMP analyses (wt%) of monazite in sample 16Slo12. The structural formula of monazite is based on four anions. For mineral abbreviations see text

Comment	In Grt_1	In O-H-I (Grt rim)		In matrix			
SiO_2	0.25	1.41	0.40	0.36	0.39	0.45	0.72
P_2O_5	29.68	27.41	28.46	28.66	27.69	29.26	28.42
SO_3	b.d.l.	b.d.l.	b.d.l.	b.d.l.	b.d.l.	0.00	b.d.l.
As_2O_5	b.d.l.	b.d.l.	b.d.l.	b.d.l.	0.02	0.00	0.00
CaO	1.35	1.15	1.04	1.13	0.85	0.76	1.02
Y_2O_3	1.76	1.20	0.06	0.04	1.85	1.58	0.17
La_2O_3	12.93	12.25	14.64	15.12	13.26	14.49	13.93
Ce_2O_3	26.51	25.64	29.47	29.83	28.59	30.69	29.68
Pr_2O_3	3.00	3.06	3.21	3.16	3.23	3.42	3.26
Nd_2O_3	10.93	11.03	11.59	10.64	13.03	12.08	11.37
Sm_2O_3	1.94	1.64	1.50	1.30	2.53	2.04	1.52
Gd_2O_3	1.73	1.24	0.67	0.55	2.10	1.50	0.55
Dy_2O_3	0.69	0.51	0.13	0.12	0.74	0.69	0.14
Er_2O_3	0.13	0.11	0.04	0.03	0.14	0.13	0.04
PbO	0.1069	0.1527	0.0260	0.0295	0.0143	0.0080	0.0062
ThO_2	6.01	10.39	5.38	5.99	4.30	4.31	6.72
UO_2	0.89	0.92	0.46	0.50	0.35	0.30	0.59
Total	97.90	98.11	97.06	97.44	99.06	101.71	98.15
Si	0.010	0.058	0.016	0.015	0.016	0.017	0.029
P	0.997	0.943	0.981	0.983	0.952	0.968	0.970
S	0.000	0.000	0.000	0.000	0.000	0.000	0.000
As	0.000	0.000	0.000	0.000	0.000	0.000	0.000
Ca	0.058	0.050	0.045	0.049	0.037	0.032	0.044
Y	0.037	0.026	0.001	0.001	0.040	0.033	0.004
La	0.189	0.184	0.220	0.226	0.199	0.209	0.207
Ce	0.385	0.382	0.439	0.442	0.425	0.439	0.438
Pr	0.043	0.045	0.048	0.047	0.048	0.049	0.048
Nd	0.155	0.160	0.168	0.154	0.189	0.169	0.164
Sm	0.027	0.023	0.021	0.018	0.035	0.027	0.021
Gd	0.023	0.017	0.009	0.007	0.028	0.019	0.007
Dy	0.009	0.007	0.002	0.002	0.010	0.009	0.002
Er	0.002	0.001	0.001	0.000	0.002	0.002	0.001
Pb	0.0011	0.0017	0.0003	0.0003	0.0002	0.0001	0.0001
Th	0.054	0.096	0.050	0.055	0.040	0.038	0.062
U	0.008	0.008	0.004	0.005	0.003	0.003	0.005
Age/Ma	285.8	271.0	90.6	93.0	63.0	36.4	17.2
1σ-error	6.5	3.6	5.4	4.9	7.9	3.8	5.2

Abbreviation: b.d.l., below detection limit.

In the *P–T* pseudosection (Figure 10a) for composition XRFA1, the staurolite+Bt_0+rutile+quartz assemblage included in the core of porphyroblastic $Grt_{0–1}$ occurs at *P–T* conditions of 600–650°C and 7.5–10.3 kbar together with potassic white mica+garnet. If kyanite (found only included in the rim of $Grt_{0–1}$) would be part of this inclusion assemblage the temperature range would be reduced to 630–650°C. The calculated garnet composition, for instance, at 8.5 kbar and 620°C is $Prp_{0.19}Grs_{0.09}$ and, thus, similar to the core composition of $Grt_{0–1}$. If we assume that the compositions of the $Grt_{0–1}$ core ($Prp_{0.23}Grs_{0.12}Sps_{0.025}$) and the highest Si content in Ph_1 (3.22 pfu) were once in equilibrium, the approach (or intersection) of the corresponding isopleths points to HP conditions ~15 kbar at

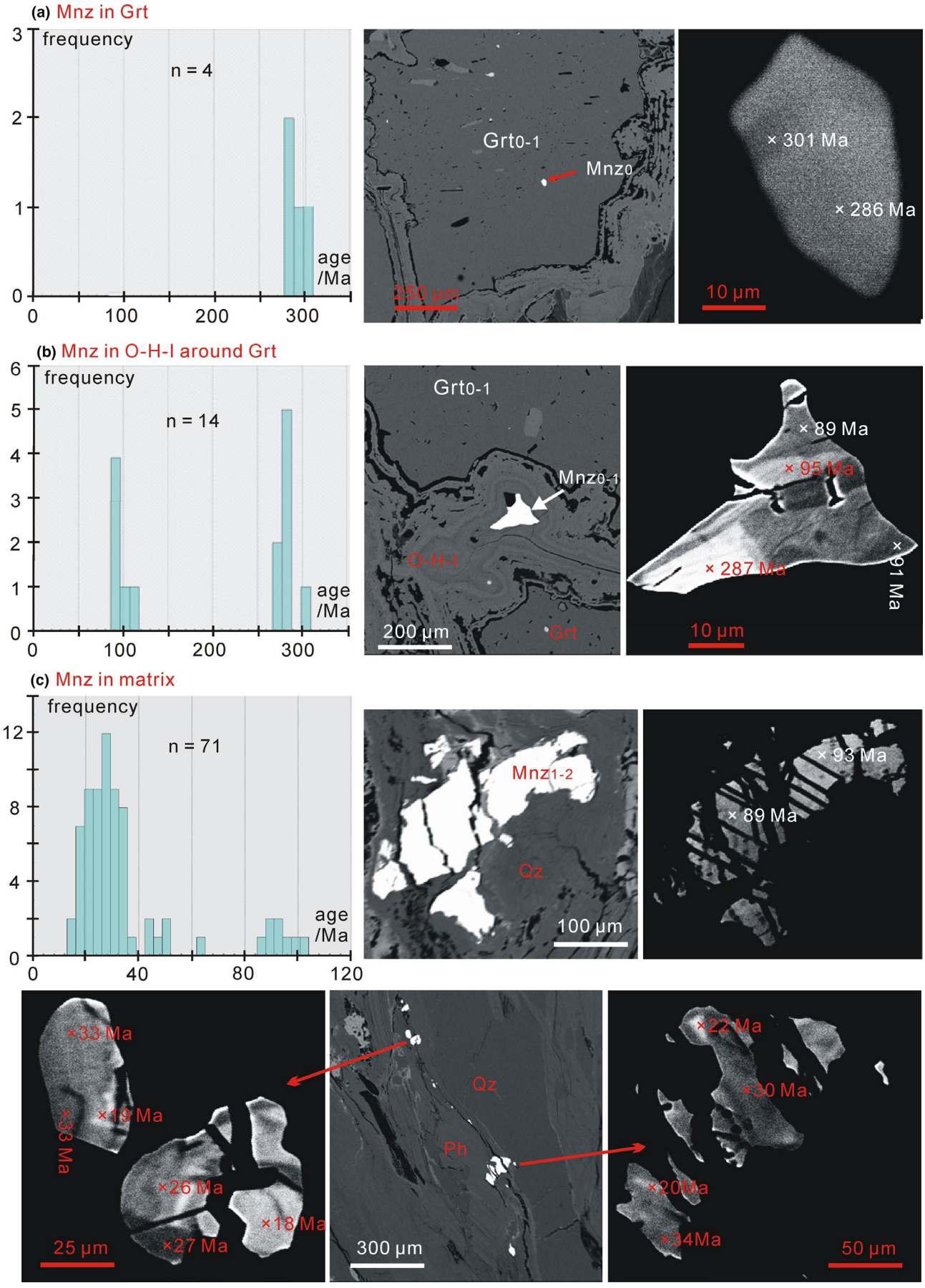

FIGURE 8 Age histograms and BSE images (metapelite 16Slo12) for monazite in garnet (a), an undefined iron hydroxide-rich mass (O-H-I) (b), and the matrix (c). For mineral abbreviations see text

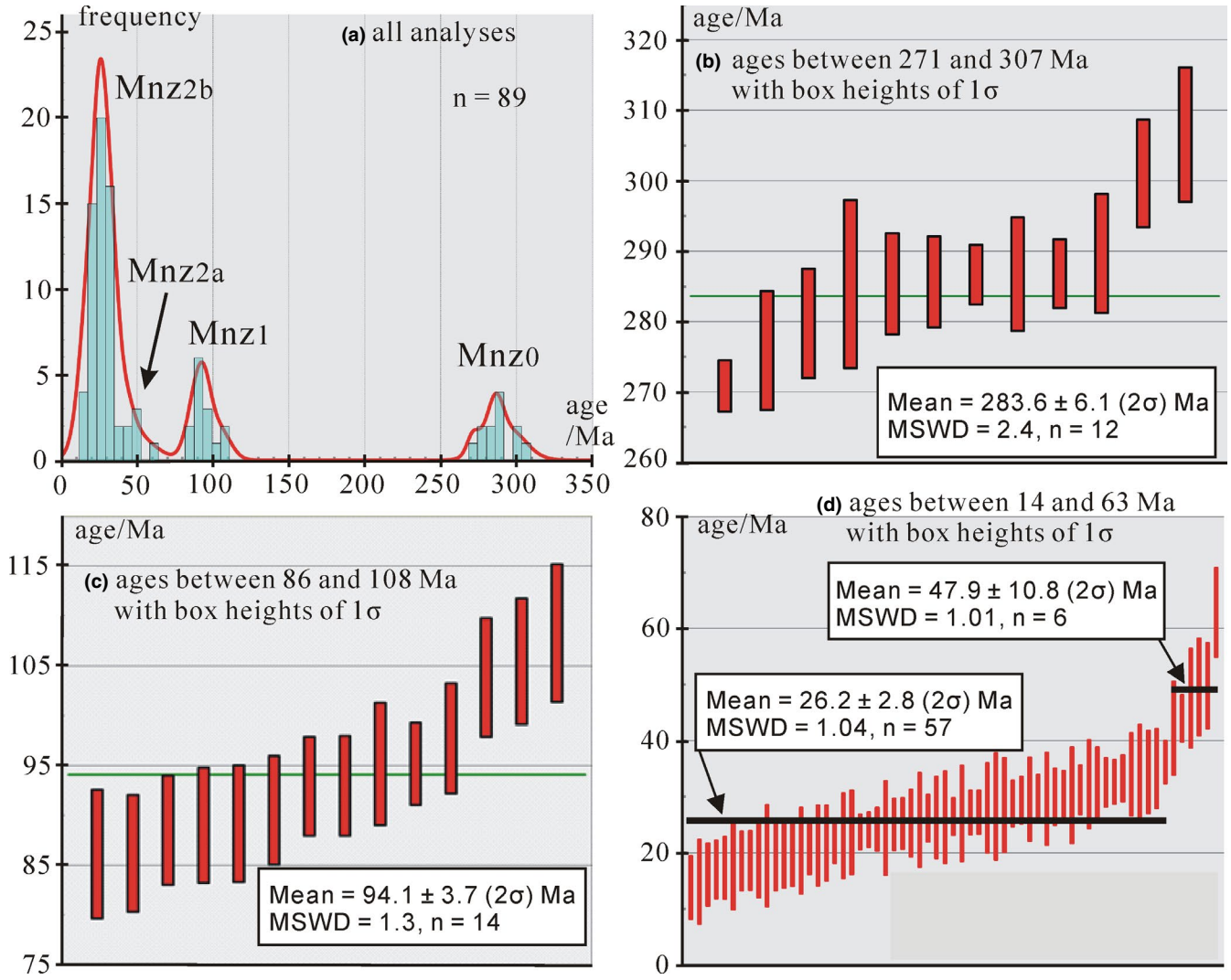

FIGURE 9 (a) Age histogram related to all monazite analyses in metapelite 16Slo12 except those four with high Th/U ratio (Figure 7a). Four age populations are discernable (see also Figure 7). (b–d) Ages of the late Variscan (b), Eo-Alpine (c), and two Tertiary populations (d). The data with 1σ error bars are arranged with increasing age to the right-hand side

575–645°C (Figure 10e). Slightly higher temperatures result if we relate this phengite composition to Grt_1. If we consider the isopleths for Grt_1 ($Prp_{0.24}Grs_{0.12}Sps_{0.012}$) and Si contents of Ph_1 lower than 3.22 (see Figure 6) a bundle of intersections occurs in the *P–T* range of 570–640°C and 8.3–15.0 kbar (Figure 10f). The isopleth (Figure S6) for the estimated modal content of porphyroblastic garnet (6 vol.%) is compatible with this *P–T* range. The calculated mineral assemblages in the given *P–T* ranges are phengite+garnet+paragonite+kyanite+rutile+quartz±chlorite±chloritoid±staurolite and phengite+garnet+rutile+quartz±kyanite±paragonite±staurolite±chlorite±chloritoid (Figure 10a).

P–T conditions of 575–620°C at 18.5–23 kbar (Figure 11) were determined for the coexistence of Grt_2 based on the garnet compositions $Prp_{0.16}Grs_{0.09}Sps_{0.012}$ (core) and $Prp_{0.14}Grs_{0.11}Sps_{0.039}$ (rim), the highest Si content in Ph_2 (3.27 pfu), and an EBC (Table 1: AEBC) obtained after applying strategy A and subtracting porphyroblastic garnet (Grt_{0-1}, Grt_1) and the early generation of potassic white mica (Ph_1). The calculated mineral assemblage at these conditions is phengite+chloritoid+garnet+kyanite+rutile+quartz.

6.3 | Zr-in-rutile and Ti-in-biotite geothermometry

For the geothermometric application of the Zr contents in rutile, we used the calibration by Tomkins et al. (2007), because this calibration considers the influence of both temperature and pressure on the Zr content in rutile. We found rutile in the porphyroblastic garnet and in O-H-I (garnet rim before alteration), but not in the matrix. Rutile, enclosed in garnet with a size of up to 70 × 20 μm^2, is elongated or subrounded showing subhedral forms whereas rutile in O-H-I is anhedral with a size of ~20 × 40 μm^2.

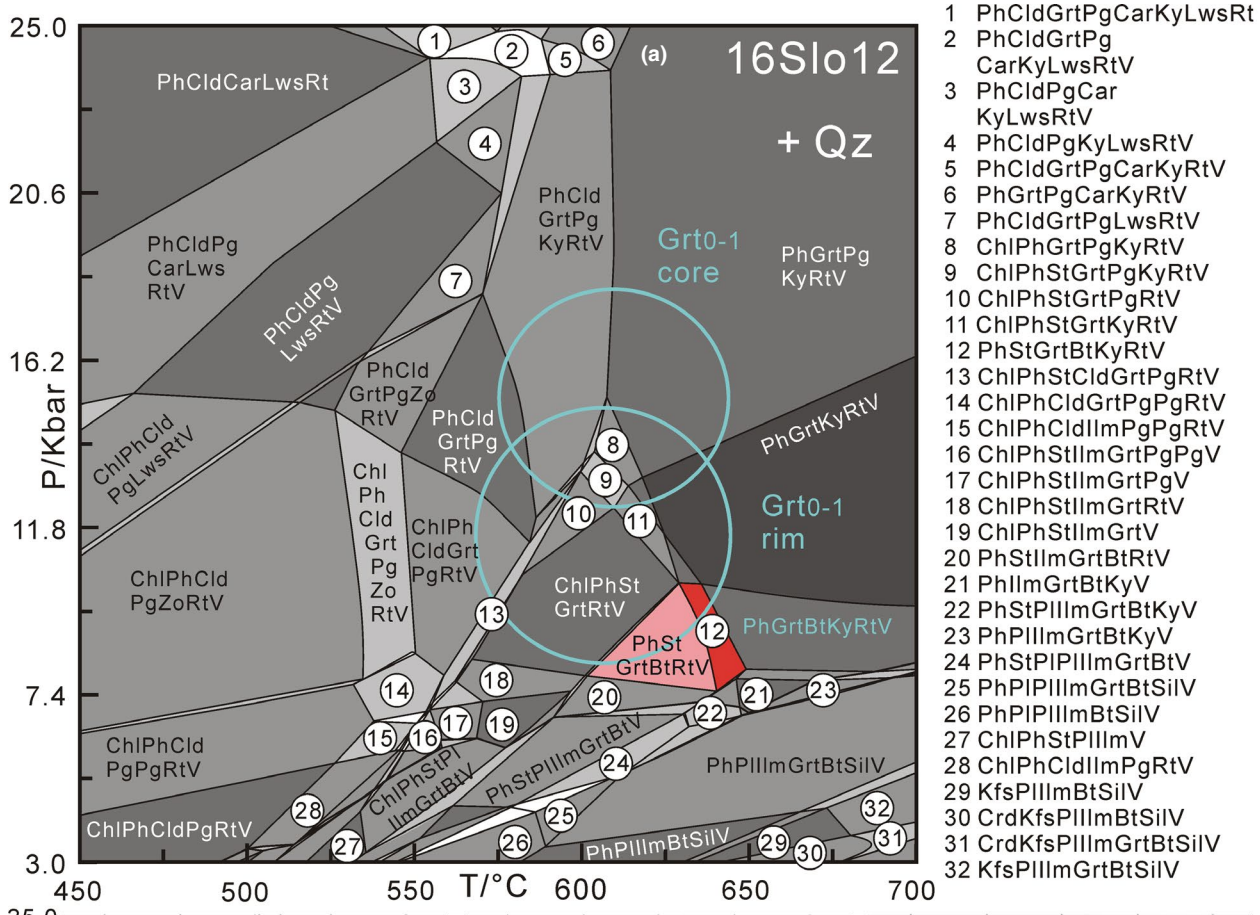

1 PhCldGrtPgCarKyLwsRt
2 PhCldGrtPg CarKyLwsRtV
3 PhCldPgCar KyLwsRtV
4 PhCldPgKyLwsRtV
5 PhCldGrtPgCarKyRtV
6 PhGrtPgCarKyRtV
7 PhCldGrtPgLwsRtV
8 ChlPhGrtPgKyRtV
9 ChlPhStGrtPgKyRtV
10 ChlPhStGrtPgRtV
11 ChlPhStGrtKyRtV
12 PhStGrtBtKyRtV
13 ChlPhStCldGrtPgRtV
14 ChlPhCldGrtPgPgRtV
15 ChlPhCldIlmPgPgRtV
16 ChlPhStIlmGrtPgPgV
17 ChlPhStIlmGrtPgV
18 ChlPhStIlmGrtRtV
19 ChlPhStIlmGrtV
20 PhStIlmGrtBtRtV
21 PhIlmGrtBtKyV
22 PhStPlIlmGrtBtKyV
23 PhPlIlmGrtBtKyV
24 PhStPlPlIlmGrtBtV
25 PhPlPlIlmGrtBtSilV
26 PhPlPlIlmBtSilV
27 ChlPhStPlIlmV
28 ChlPhCldIlmPgRtV
29 KfsPlIlmBtSilV
30 CrdKfsPlIlmBtSilV
31 CrdKfsPlIlmGrtBtSilV
32 KfsPlIlmGrtBtSilV

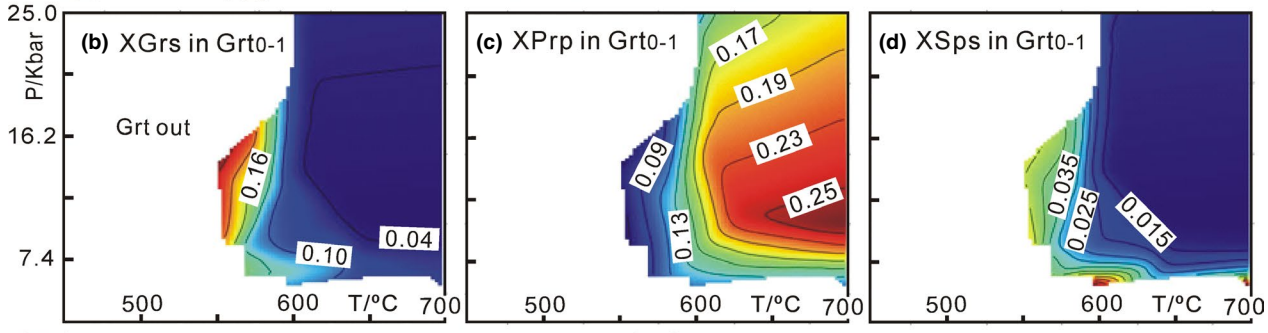

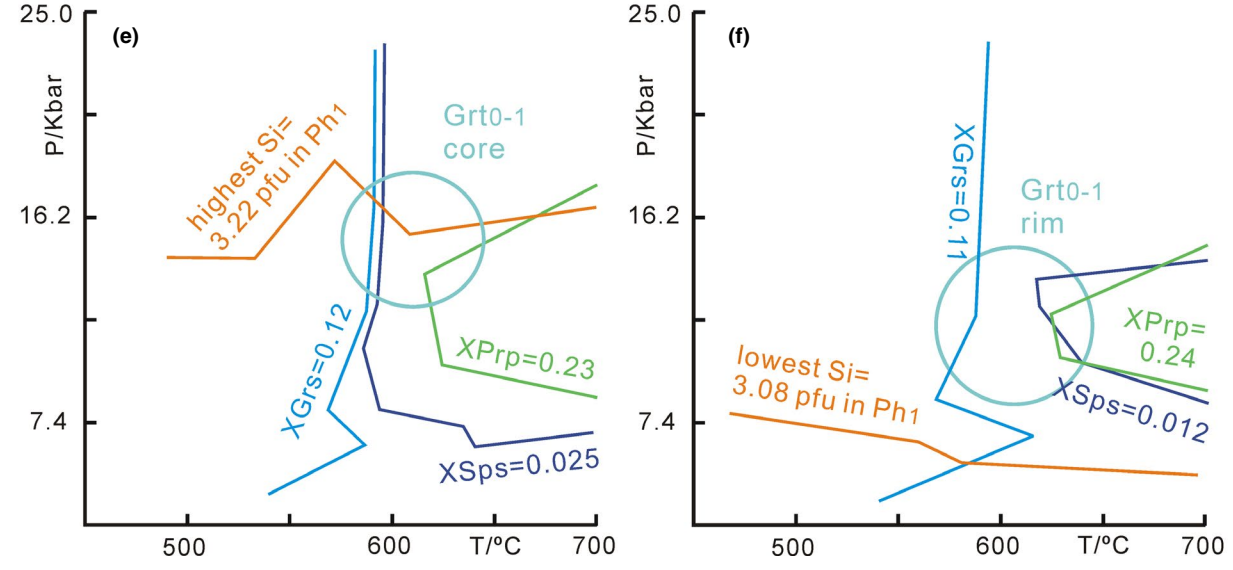

FIGURE 10 (a) *P–T* pseudosection for sample 16Slo12 calculated for its bulk–rock composition (Table 1—XRFA1) with PERPLE_X (thermodynamic data set 1). Pink and red areas are consistent with the inclusion assemblages in $Grt_{0–1}$ core and rim respectively. (b–d) Contouring of the pseudosection by isopleths for molar fractions of garnet components using program PyWerami created by Ondrej Lexa, Czech Geological Survey (see https://petrol.natur.cuni.cz/~ondro/oldweb/pywerami:home). (e) Peak-pressure conditions (within the cyan circle with a higher probability in the central region than closer to the margin) were tentatively deduced from the composition of the porphyroblastic garnet core ($Grt_{0–1}$) and the highest Si content in Ph_1. (f) *P–T* conditions (within the cyan circle) were estimated from the composition of the porphyroblastic garnet rim (= Grt_1). For mineral abbreviations see text

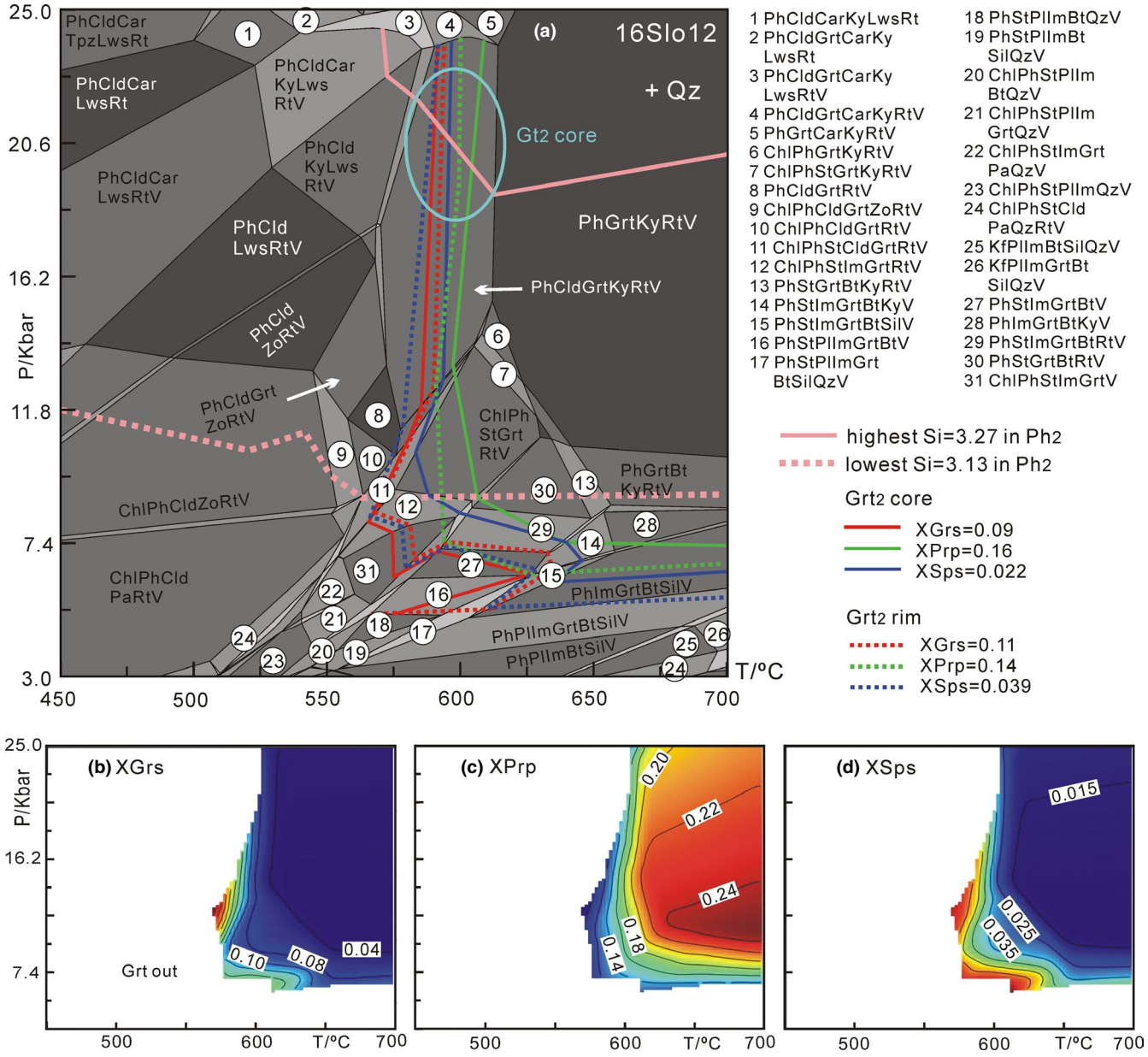

FIGURE 11 (a) *P–T* pseudosection for sample 16Slo12 calculated for its slightly oxidized bulk-rock composition (AEBC in Table 1) with PERPLE_X (thermodynamic data set 1). *P–T* conditions (cyan circle represents an assumed 2σ error range) were deduced from the composition of small garnet (Grt_2) and the highest Si content in Ph_2. (b–d) Contouring of the pseudosection by isopleths for molar fractions of garnet components using program PyWerami (see Figure 10). For mineral abbreviations see text

Twenty-six rutile grains enclosed in garnet were analysed by 46 spot analyses. In addition, five grains, that are surrounded by O-H-I, were investigated by 12 spot analyses. In BSE images no compositional zoning of rutile was recognized. The Zr contents in all grains are in a narrow range of 180–290 ppm resulting in temperatures ~620 ± 9 (1σ)°C at 7.5 kbar and 630 ± 9°C at 10.3 kbar. The applied pressures refer to the lowest and highest ones of the *P–T* range assigned

to inclusions in porphyroblastic garnet (Figure 10a). The calculated temperatures are consistent with the temperatures (600–650°C) derived above for the inclusion assemblage in porphyroblastic garnet (Figure 10a).

The Ti-in-biotite thermometer calibrated by Henry et al. (2005) is pressure independent and suitable for biotite characterized by *X*Mg between 0.275 and 1.0 and Ti contents between 0.04 and 0.60 pfu. This thermometer should be applied to metamorphosed sedimentary rocks which are ilmenite- or rutile-bearing, graphitic and peraluminous. Thus, it can be applied to biotite (*X*Mg = 0.72–0.76, Ti = 0.05–0.095 pfu) enclosed in garnet of sample 16Slo12. Although Henry et al. (2005) mentioned that their calibration of the Ti-in-biotite thermometer is most suitable for temperatures between 480 and 800°C and pressures between 3 and 6 kbar, these authors also suggest that this thermometer can be used for higher pressures than 6 kbar.

Twenty-six analyses of Bt_0 gave temperatures between 546 and 667°C with an average of 619 ± 28.5°C (Figure S7). The obtained average temperature is consistent with the result of the Zr-in-rutile thermometry for the inclusion assemblage in Grt_0.

6.4 | Intracrystalline diffusion in garnet and its possible influence on *P–T* estimates

As extended domains of porphyroblastic garnet (core of $Grt_{0–1}$, Grt_1, see Figure 5) are nearly chemically homogeneous, the question arises if homogenization by intracrystalline cation diffusion occurred and, thus, had an influence on the previously reported *P–T* estimates. Commonly, this diffusion is insignificant in garnet unless temperatures of 650–700°C are exceeded which is not the case here. However, it is possible that very long residence times at temperatures of 650°C or somewhat lower are responsible for both nearly homogeneous garnet domains (core of $Grt_{0–1}$ = Grt_0, Grt_1). To test this possibility, we have modelled the compositional change of garnet by intracrystalline cation diffusion with the DXL program by Perchuk and Gerya (2005) using version 7.5 and diffusion data by Perchuk et al. (2009). For Grt_0, we assumed (a) a maximum residence time (Figure 12a), which is, according to our monazite dating (Section 5), *c*. 180 Ma, the age difference between the Permian and the beginning of the Eo-Alpine metamorphic events, and (b) a permanent exposure to a high temperature of 630°C, which can be considered as being somewhat above the average resulting from the two types of geothermometry applied (Section 6.3), the *P–T* location of garnet isopleths above 9 kbar (Section 6.2), and lacking indications for melting ($T < 670$°C). Furthermore, we started with a garnet growth profile that was reconstructed for a prograde path to 9.5 kbar and 630°C as shown in Figure 12a. For this purpose, we applied a simplified version of the method by Konrad-Schmolke et al. (2008) as reported in detail by Massonne and Li (2020). This method requires the application of an EBC that was calculated after a small growth zone of garnet had formed (by subtraction of this growth zone from the previously used EBC).

Two slightly different chemical profiles were determined for a garnet of 2 mm diameter (after final growth) that has formed along the *P–T* path shown in Figure 12a. One profile (Figure 12b) was reconstructed, without consideration of EBCs, using the werami subprogram of PERPLE_X (Connolly, 2005) for the data obtained by computing the pseudosection shown in Figure 10. For the other garnet profile (Figure 12c) a sequence of seven different EBCs were additionally applied (the corresponding xls-file with the underlying calculation scheme is available on request). Both obtained garnet profiles are bell-shaped (*X*Grs, *X*Sps) with a stronger fractionation of Ca and Mn in the profile considering EBCs. Somewhat more than 80% of the profile length of garnet (Grt core = Grt_0) is caused by temperature increase to 630°C (66% of the entire garnet volume in the calculation without an EBC, 48% with EBCs). The garnet rim (Grt_1) forms by pressure increase to 11 kbar (without an EBC) or 15 kbar (with EBCs) and is characterized by a nearly constant composition caused by staurolite breakdown (~10.5 kbar, without an EBC; close to 13 kbar, with EBCs). No further growth of garnet was calculated above 11 kbar (or 15 kbar, with EBCs) despite the assumed slight increase in temperature after reaching the pressure climax of 16 kbar (Figure 12a). The lack of growth of garnet before reaching the metamorphic peak was also noted by Brouwer et al. (2005), Štípská and Powell (2005), and Massonne and Li (2020) depending on the course of the *P–T* trajectory.

Although the disadvantage of the DXL program is the simulation of intracrystalline cation diffusion (a three-dimensional process in nature) along a one-dimensional profile only, it is obvious that no significant change of the constructed garnet profiles occurs by this diffusion (see example in Figure 12d) despite the selected long-lasting exposure to relatively high temperatures. Thus, our *P–T* estimates reported in Section 6.2 are not disturbed by intracrystalline cation diffusion in garnet.

We have also modelled the change by diffusion after garnet has formed by two growth pulses leading to chemically homogeneous Grt_0 and Grt_1 (see Section 7.3 below). The sharp contact of these garnet domains will turn to an almost 200 μm wide transition zone after 60 Ma of diffusion at the selected average temperature of 640°C (Figure 12e).

7 | DISCUSSION

7.1 | Age constraints

In this study, monazite records three major metamorphic events in Permian, 283.6 ± 6.1 (2σ) Ma, Eo-Alpine,

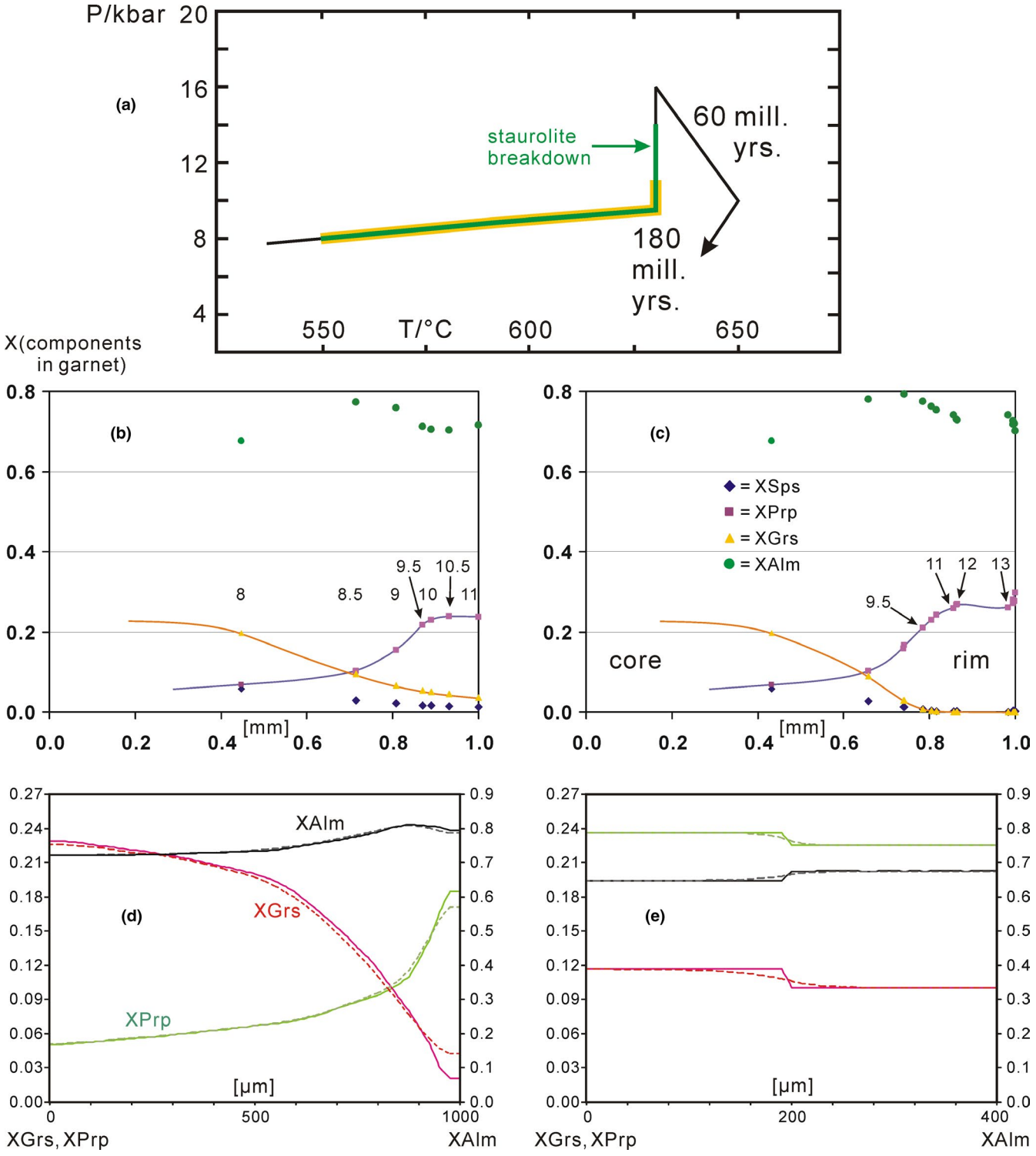

FIGURE 12 Calculated chemical profiles of garnet (a–c) and change (d, e) by intracrystalline cation diffusion. (a) *P–T* path considered for the construction of these profiles (see text). The yellow and green branches of this path mark prograde growth of garnet concerning the profile in (b) and (c) respectively. (b) Calculated chemical profile from core to rim of a garnet with 2 mm diameter in terms of molar fractions of almandine (*X*Alm), grossular (*X*Grs), pyrope (*X*Prp) and spessartine (*X*Sps) components. For this profile the garnet compositions (see symbols) were only calculated at certain *P–T* conditions (only *P* is given in kbar) applying the same data used for the construction of the *P–T* pseudosection of Figure 10. The profile lines for *X*Grs and *X*Prp were hand-drawn passing through the corresponding symbols (c) As (b) but the calculation considered a sequence of seven EBCs. (d) Profile for Grt_0 (as in b with the simplification *X*Alm = 1−(*X*Grs+XPrp), solid lines) after intracrystalline cation diffusion at 630°C and 180 Ma (broken lines) using the DXL program (profile subdivided in 40 equal steps, *P* = 9 kbar). (e) Profile through the contact of assumed chemically homogeneous Grt_0 (core of Grt_{0-1}, for composition see Table 2) and Grt_1 (rim of Grt_{0-1}) at *t* = 0 (solid lines) and after 60 Ma cation diffusion at 640°C (broken lines) calculated with DXL (profile subdivided in 40 equal steps, *P* = 12 kbar).

94.1 ± 3.7 Ma, and Tertiary times (Figure 9). The Eo-Alpine metamorphic event is compatible with reported ages (mostly 90–93 Ma) for diverse rocks in the Pohorje nappe, using different dating techniques (see Geological setting). Unlike the Eo-Alpine population, our oldest population has not received much attention so far in the study area. Only zircon cores in metapelite of the Pohorje Mts. with Permian (286 and 258 Ma)–Triassic (238 Ma) U–Pb ages were reported by Janák et al. (2009), who also related these ages to an orogenic event experienced by the metapelite. In the adjacent Koralpe–Saualpe terrane to the northwest, late Variscan metamorphic ages have been repeatedly reported (Habler & Thöni, 2001; Miller & Thöni, 1997; Morauf, 1981; Schulz, 2017; Tenczer et al., 2006; Thöni & Miller, 1996, 2009) in addition to Eo-Alpine ages. Thus, it is undoubtful that our oldest population of 284 Ma refers to a metamorphic event especially since the corresponding monazite is enclosed in the same garnet domain as the inclusion assemblage with staurolite.

The Tertiary monazite, yielding populations at 47.9 ± 10.8 and 26.2 ± 2.8 (2σ) Ma (Figure 9d), does not support the decompression metamorphism at 76 ± 16 Ma proposed by Krenn et al. (2009) on the basis of U–Th–Pb monazite ages which were obtained also on metapelite from the Pohorje Mts. We interpret our population at 48 Ma as the result of an Eocene burial (see also below). Metamorphism accompanied by exhumation occurred close to the turn to the Late Tertiary according to our population at 26 Ma. The idea that our Tertiary ages were caused by nearby intrusions of tonalite–granodiorite must be abandoned because of two main reasons: (a) the magma intrusions occurred in the Burdigalian (Fodor et al., 2008; Trajanova et al., 2008) and, thus, significantly later than the youngest of both Tertiary ages determined on monazite and (b) a possible resetting of older monazite ages (Permian, Eo-Alpine) by heat and fluids generated by the voluminous Miocene intrusions in the Pohorje cannot result in the observed geochemical systematics of monazite (Figure 7, see the Tertiary high-Y monazite that is older than the Oligocene low-Y monazite). In addition, an Oligocene HP event is compatible with an exhumation stage at 18.6 Ma (Fodor et al., 2008) at which the exposed Pohorje tonalite–granodiorite body intruded a crustal level corresponding to 7 kbar (Altherr et al., 1995). Further exhumation and cooling was noted to have occurred in the time interval 10–19 Ma based on K–Ar dating on micas in metamorphic rocks from the Pohorje Mts. (Fodor et al., 2002) and the fission-track method on apatite from a gneiss of the eastern slope of the Pohorje Mts. (Sachsenhofer et al., 1998).

7.2 | Correlation between monazite ages and growth of garnet

In order to better relate the above monazite age episodes to the metamorphic evolution, one of the most widely used approaches is to link monazite formation and garnet growth/dissolution (Mottram et al., 2014; Regis et al., 2016; Wang et al., 2015; Williams et al., 2007). Since garnet is a major phase, relatively rich in Y and heavy rare-earth elements (HREE), its growth/dissolution affects the trace element composition of monazite. Monazite growing in the presence of garnet can only incorporate relatively low Y contents whereas monazite forming in the absence of garnet or during garnet breakdown incorporates relatively high Y contents (Kohn et al., 2005; Massonne, Cruciani, et al., 2018; Pyle & Spear, 2003; Pyle et al., 2001). A reduced introduction of HREE (similar to Y) in monazite (Hacker et al., 2015; Hermann & Rubatto, 2003; Rubatto et al., 2006) can be seen by relatively high molar or mass ratios of La/Gd (Massonne, 2014, 2016; Massonne, Cruciani, et al., 2018) for monazite analysed with the EMP.

Our monazite populations show clearly distinct Y contents and La/Gd ratios. The oldest population (284 Ma) is characterized by relatively high Y contents (~1.15 wt% Y) and low La/Gd ratios (8.7, Figure 7). Thus, we conclude that this monazite population formed before the growth of the porphyroblastic garnet in the studied metapelite compatible with the inclusion of this monazite in this garnet and its O-H-I alteration product (Figure 13). The Eo-Alpine population of monazite, however, grew synchronously with (or after) porphyroblastic garnet, due to the low Y contents (~0.05 wt%) and high La/Gd ratios (21.4, Figure 7). The older Tertiary population (48 Ma) shows again high Y contents (1.1 wt%) and low La/Gd ratios (10.6, Figure 7b,c). Consequently, such monazite must have grown after the corrosion of the porphyroblastic garnet (Figure 13), concluded from the shape of this garnet (+ O-H-I), and before Grt_2. The younger Tertiary population is characterized by a spread of both Y contents (0.0–1.4 wt%) and La/Gd ratios (6.1–32.1, Figure 7b,c). This could mean that monazite of this population grew partly before and after formation of Grt_2 within a narrow time interval that cannot be resolved with the EMP dating method. Therefore, we

FIGURE 13 Sketch showing the (assumed) texture (left hand side) of monazite, garnet and other rock-forming minerals in sample 16Slo12 at different metamorphic stages (+weathering) and the relation to *P–T* paths (right hand side). The texture sketch for the Eo-Alpine is that of a medium-grained micaschist that refers to the end of the solid Eo-Alpine *P–T* path (box adjacent to the right with the cyan path the more likely one compared to the red path as mentioned in the text). In the texture sketch for the Tertiary event, garnet is tentatively distinguished by three different pink colours (light to dark) to mark its various growth stages. The texture in this sketch refers to the end of the solid Tertiary *P–T* path. The texture sketch at the bottom is that of Figure 4. For mineral abbreviations see text

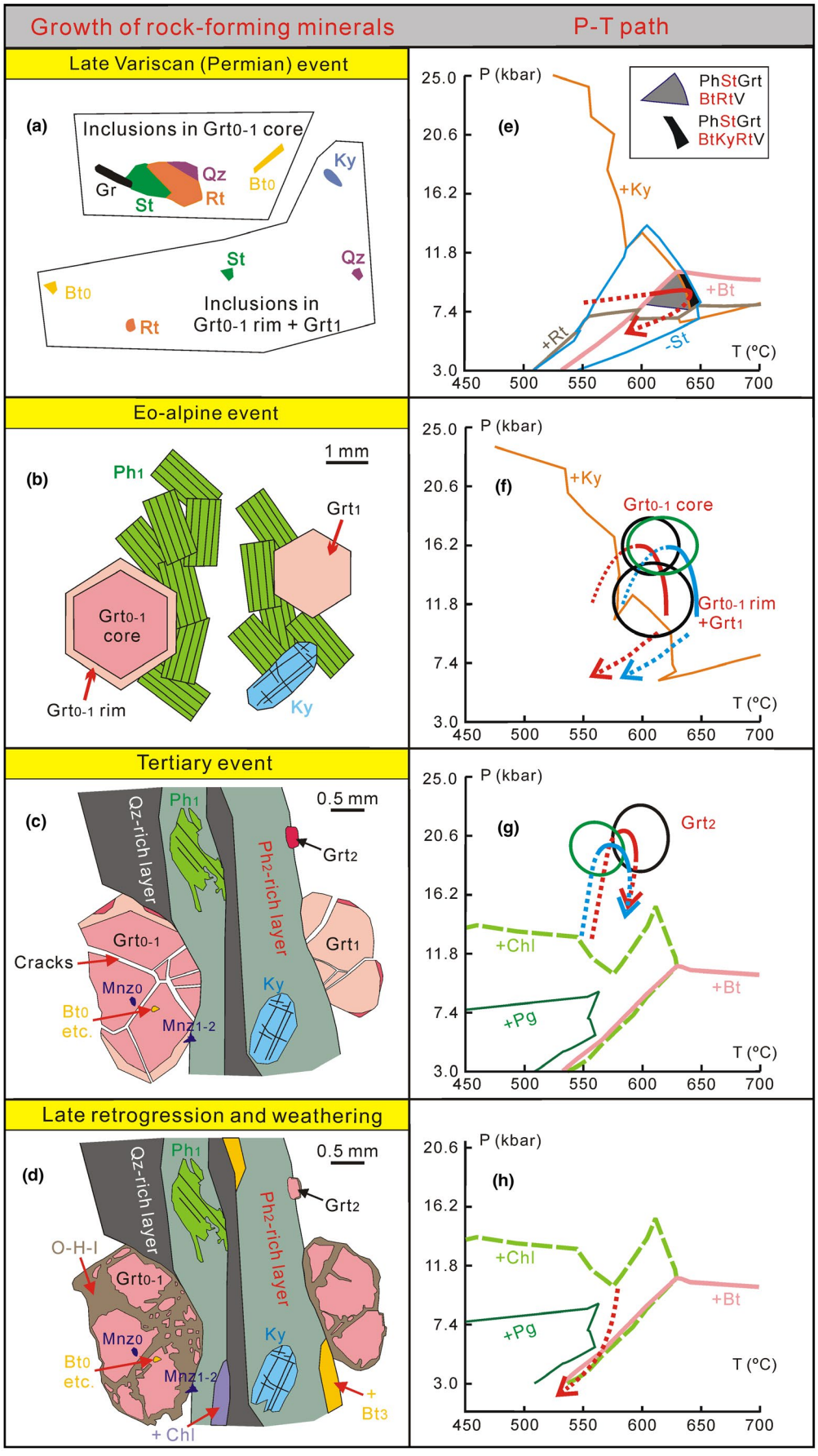
Growth of rock-forming minerals
P-T path
Late Variscan (Permian) event
(a)
Inclusions in Grt0-1 core
Gr
St
Qz
Rt
Bt0
Ky
St
Qz
Bt0
Rt
Inclusions in
Grt0-1 rim + Grt1
(e)
P (kbar)
T (°C)
PhStGrt
BtRtV
PhStGrt
BtKyRtV
+Ky
+Bt
+Rt
-St
Eo-alpine event
(b)
1 mm
Ph1
Grt1
Grt0-1
core
Grt0-1 rim
Ky
(f)
+Ky
Grt0-1 core
Grt0-1 rim
+Grt1
Tertiary event
(c)
0.5 mm
Qz-rich layer
Ph1
Ph2-rich layer
Grt2
Grt0-1
Grt1
Cracks
Mnz0
Bt0
etc.
Mnz1-2
Ky
(g)
Grt2
+Chl
+Bt
+Pg
Late retrogression and weathering
(d)
0.5 mm
Qz-rich layer
Ph1
Ph2-rich layer
Grt2
O-H-I
Grt0-1
Mnz0
Bt0
etc.
Mnz1-2
Ky
+
Bt3
+ Chl
(h)
+Chl
+Bt
+Pg

relate the mean age of 26 Ma to a period between the HP conditions at which Grt_2 formed (see below) and early exhumation during the Tertiary metamorphic cycle.

7.3 | *P–T* evolution

Polymetamorphism in the Pohorje Mts. is revealed by different generations of monazite and two (or three) generations of garnet and phengite in the studied micaschist and, thus, assigned to Permian, Eo-Alpine and Tertiary metamorphic events (see also above). Concerning the *P–T* conditions related to these events, the not well-definable original bulk-rock composition owing to weathering and precipitation of O-H-I caused problems in the establishment of relatively accurate estimates. We prefer (see above) to use the results obtained by PERPLE_X with EBCs XRFA1 and AEBC and thermodynamic data set 1 and the Zr-in-rutile and Ti-in-biotite thermometry. However, we are aware that, using these thermobarometric methods, a slight temperature underestimation might has been eventuated for the formation of Grt_1 due to corresponding isopleths for XPrp located at higher temperatures when performing PERPLE_X calculations with compositions XRF1 and XRFB1. On the other hand, a slight temperature overestimation might have occurred for the formation of Grt_2 because the application of thermodynamic data set 2 yielded somewhat lower temperatures for this formation than thermodynamic data set 1. The peak pressure estimates, however, are hardly affected as they are based on chemical compositions of phengite the barometry with which is well established and not sensitive for the range of bulk-rock compositions and thermodynamic data sets used here.

7.3.1 | Permian evolution

In fact, no *P–T* path could be derived for the earliest metamorphic event, but due to the inclusion assemblage of gra phite+staurolite(+kyanite?)+biotite+rutile+quartz+Perm ian monazite in porphyroblastic garnet, a *P–T* range of 7.5–10.3 kbar and 600–650°C, compatible with the applied Zr-in-rutile and Ti-in-biotite thermometry, and a reduced (low f_{O2}) environment can be defined. These *P–T* data are broadly compatible with a regional Permian high-temperature–low-pressure (HT–LP) event in the Austroalpine realm proposed by several authors (e.g. Gaidies et al., 2008; Schuster et al., 2001; Schuster & Stüwe, 2008) including the Pohorje and the adjacent Koralpe–Saualpe terrane (Krenn et al., 2012; Schulz, 2017; Tenczer et al., 2006). A high probability exists that the core of Grt_{0-1} has already formed during the Permian metamorphic event as its composition ($Prp_{0.23}Grs_{0.12}Sps_{0.025}$) is compatible with the derived *P–T* range of 7.5–10.3 kbar and 600–650° (Figure 10e). This nearly homogeneous composition originated by a growth pulse of garnet after (or during) the inclusion assemblage had formed. The alternative explanation, a growth zonation and subsequent intracrystalline cation diffusion in garnet during a very long residence time at relative high temperatures to homogenize this zonation, was examined in detail, and shown to be unlikely, in Section 6.4 (Figure 12d) and could not explain the inclusions, formed above 600°C, in the inner garnet core. In any case (Permian or Eo-Alpine), the growth of garnet started clearly within its *P–T* field (see Figures 10 and 11 and Figures S2–S5) and not soon after crossing the boundary to this field during prograde metamorphism. The overstepping of this boundary is explained by kinetic factors (energetic barriers) as outlined by Spear (2017). Significant *P–T* differences (up to 10 kbar and 100°C) between beginning of garnet growth and crossing the garnet-in boundary are possible (see Castro & Spear, 2017; Li et al., 2017, 2020; Spear et al., 2014). The consequence of the overstepping phenomenon is a growth pulse leading to (nearly) chemically homogeneous, large garnet grains with abundant inclusions as observed in sample 16Slo12.

7.3.2 | Eo-Alpine evolution

The subsequent metamorphic event occurred in Eo-Alpine times (monazite population at 94 Ma). According to the above assumption that the chemical compositions of Grt_1 (or Grt_0 if the Grt_{0-1} core would not have formed in the Permian) and the early generation (highest Si contents) of phengite (Ph_1) would have coexisted (Figures 6 and 13), the metapelite reached peak pressures of 12.3–18.2 kbar in the temperature range 575–645°C (Figures 10e and 13 and Figures S2e and S3e) with the highest temperatures of this range being most likely (see above). However, our reconstruction of the garnet growth zonation in Section 6.4 (Figure 12b,c) has demonstrated that garnet grew further by a second pulse (Grt_1), this time not by overstepping but by breakdown of staurolite, relicts of which are preserved as inclusions in Grt_0. The corresponding reaction occurs in the pressure range 11–13 kbar, depending on the not perfectly known EBC and temperature, and, thus, at higher pressures than derived for the Permian event. This suggested range could mean that the pressure derived from the maximum Si content in potassic white mica was somewhat overestimated (e.g. due to imperfect EMP analytics), but we prefer the possibility that the Ph_1 core has crystallized after Grt_1, so that the peak pressure of the Eo-Alpine event was rather 16 ± 2 kbar (Figure 10e). Temperatures at this stage were above 600°C to account for the observed garnet mode (Figure S6, minimum 6 vol.%, see subsequent section). In addition, such a high temperature, maintained to the beginning of the Tertiary event discussed below, could be responsible for the transition zone between Grt_0 and Grt_1 as suggested by diffusion modelling (Figure 12e).

It is probable that a period of nearly isothermal exhumation followed. Such an exhumation path is reflected by the decrease in the Si content in Ph_1 from core regions towards the rim. The lowest pressure reached during this exhumation might be rather ~6 kbar (see Figure 10f and Figures S3f, S4f) considering the mean of the cluster of low-Si Ph_1 (Figure 6) of 3.08 Si pfu.

Our deduced peak-pressure conditions ~16 kbar for the Eo-Alpine event are within errors compatible with *P–T* estimates by Herg and Stüwe (2018) for HP micaschists from the Plankogel unit, located between Pohorje and Koralpe–Saualpe terrane, to the Pohorje. Sample AH13 of these authors, taken ~9 km west of our micaschist sample 16Slo12, yielded a peak pressure of 17.5 kbar, calculated for an assumed temperature of 700°C. Eo-Alpine garnet in polymetamorphic micaschist from the Eclogite Unit, situated directly below the Plankogel unit (Herg & Stüwe, 2018; Schorn & Stüwe, 2016), in the Saualpe area formed at ~15 kbar and 700°C (Schulz, 2017). A garnet–kyanite-bearing gneiss in the Eclogite Unit of this area experienced peak *P–T* conditions of 18 kbar and 685°C (Thöni & Miller, 2010). However, this temperature as well as 700°C estimated by Schulz (2017) is higher than the maximum temperature of ~650°C considered for sample 16Slo12 at the Eo-Alpine peak pressure.

The here derived Eo-Alpine peak–pressure conditions contradict those for metasediments (22–27.5 kbar, 700–800°C), reported by Krenn et al. (2009), Hurai et al. (2010), and Janák et al. (2009), and eclogite, peridotite and metapelite (30–40 kbar, 700–940°C), published by Hauzenberger et al. (2016), Janák et al. (2004, 2006, 2015), and Vrabec et al. (2012) in the Pohorje Mts. (Figure 14). The *P–T* contrast between the here studied metapelite and, on the other hand, peridotite and eclogite could have resulted from a specific tectonic scenario (see also below) as was invoked for other metamorphic areas where such a contrast was noted as well (e.g. Braga et al., 2007; Li & Massonne, 2016; Štípská et al., 2012; Willner et al., 2000). But particularly the pressure contrast (>20 kbar) between our finding and the UHP metapelite that was sampled by Janák et al. (2015) from the same micaschist body as in this work (Figure 1c) requires a closer inspection.

Micrometer-sized inclusions in garnet containing diamond were taken by Janák et al. (2015) as important evidence for the UHP nature of the micaschist. Recently, Farré-de-Pablo et al. (2019) reported diamond enclosed in chromite from a serpentinite body and argued for metastable formation of diamond. Although this conclusion was questioned by Massonne (2019) because of the exposure of xenomorphic diamond in opened voids, a very similar occurrence of diamond enclosed in olivine of a basic body in a Cuban ophiolite was reported by Pujol-Solà et al. (2020). These authors could demonstrate by Raman spectroscopy that xenomorphic diamond is already in voids in olivine before these were opened. This diamond formed metastably at significantly lower pressures than necessary for stable formation of diamond. In case of both diamond occurrences in basic to ultrabasic rocks, Farré-de-Pablo et al. (2019) and Pujol-Solà et al. (2020) argued that the voids containing xenomorphic diamond were previously filled with a $CO_2 + CH_4$ fluid which can be extremely reducing. Such a fluid, that has filled the inclusions in garnet in which diamond was found by Janak et al. (2015), was reported by Hurai et al. (2010). After opening, these inclusions showed xenomorphic diamond, cavities (after the fluid has escaped) and, in some instances, moissanite (SiC)

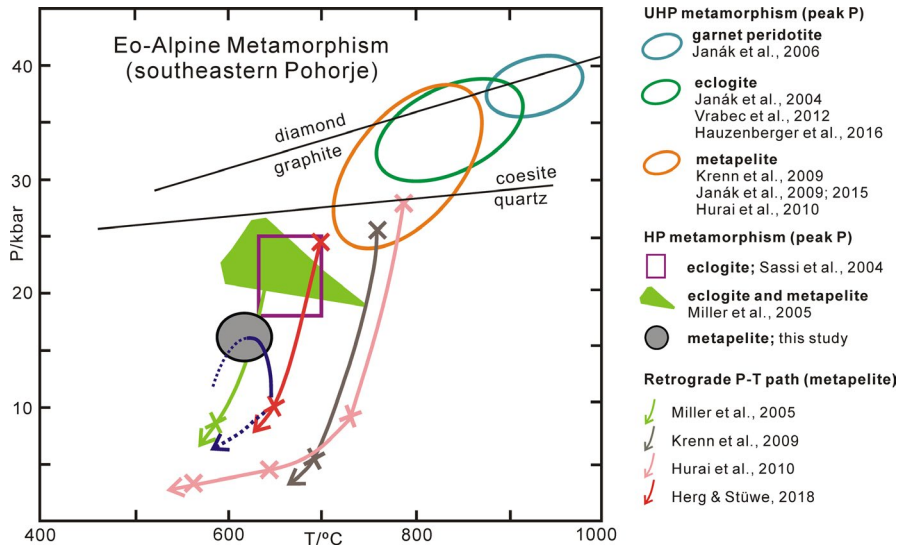

FIGURE 14 Comparison of the here obtained (blue curves, see Figure 13) and previously reported (see legend) Eo-Alpine *P–T* paths for metamorphic rocks from the southeastern Pohorje Mountains. The diamond-graphite and coesite-quartz transition curves are from Day (2012) and Massonne (1999) respectively. Note that the retrograde paths for metapelites were partially drawn by the present authors using *P–T* information (crosses) given by the corresponding authors mentioned in the legend

which could have formed because of the extremely reducing behaviour of the CO_2 + CH_4 fluid (Pujol-Solà et al., 2020). Given the similarity (fluid, xenomorphic diamond) with the diamond-bearing inclusions reported by Farré-de-Pablo et al. (2019) and Pujol-Solà et al. (2020), we consider it possible that the diamond in the studied metapelite body of the Pohorje Mts. also formed metastably and thus cannot be used to emphatically constrain the metamorphic peak pressure to the diamond field. Furthermore, the maximum Si content of phengite in the studied micaschist has the potential to constrain this pressure. For this purpose, we used X-ray maps to find locations where relics of phengite with maximum Si content occur. However, we did not use the maximum analyzed Si content, which yielded 3.325 pfu (Figure 6), but the average (3.27 pfu) of the Ph_2 population with high Si contents (in analogy: 3.22 Si pfu in Ph_1). The difference between 3.325 and 3.27 pfu is broadly compatible with analytical errors of ± 1% in the EMP determination of the Si content in phengite. Our treatment of phengite analyses and the assignment of Ph_2 to metamorphism that followed the Eo-Alpine event (see section 7.3.3) explains why we obtained lower peak pressures for this event than Krenn et al. (2009: 26 kbar based on 3.33 Si pfu in phengite) and Janák et al. (2009, see also Hurai et al., 2010: 24.5 kbar, 3.34 Si pfu), who had studied garnet-kyanite gneiss samples taken close to the location of 16Slo12.

Metamorphic peak temperatures for the garnet–kyanite gneisses were given ~150°C higher by Janák et al. (2009) and Krenn et al. (2009) than determined here for 16Slo12. One reason could be the overestimation of the peak pressures which usually results in an overestimation of temperature due to a positive temperature dependence on pressure of most geothermometers (here: pyrope content in garnet with isopleths showing dP/dT slopes only ~65 bar/°C in the *P–T* graphs by Janák et al., 2009 and Krenn et al., 2009). On the other hand, Hurai et al. (2010) and Janák et al. (2009) reported that the garnet–kyanite gneisses show evidence for partial melting whereas our temperature estimate (≤650°C) is compatible with the absence of indicators for melting in the studied micaschists.

7.3.3 | Tertiary evolution

The *P–T* loop in Tertiary times also led to eclogite facies metamorphism with peak–pressure conditions of 18.5–23 kbar at temperatures of 575–620°C (Figure 11 and Figures S4 and S5) based on the compositions of Grt_2 and the highest Si (3.27 pfu, Figure 6) content in Ph_2. The lowest temperatures of this range, resulting from the application of thermodynamic data set 2 (Figure S5), seem to be more likely. In this case, the temperature difference between the two HP events recorded in the studied micaschist could amount to up to 70°C. Such a difference (50–70°C) would explain why the Na content in Ph_2 is significantly lower than in Ph_1. Significantly lower peak temperatures for the Tertiary event compared to the Eo-Alpine event should not result in additional growth of garnet (Grt_2) and, thus, increased garnet modal content (Figure S6, altogether ~12 vol.% before replacement by O-H-I). We assume that the partial re-equilibration of the minerals (Grt_2 growth at the expense of $Grt_{0–1}$) in the studied rock to the HP conditions of the Palaeogene metamorphism was facilitated by a deformational event. The strength of this event was rather moderate than strong as the relatively coarse-grained mica flakes, formed during the Eo-Alpine event, are partially preserved (Figures 2c and 13). However, the tectonic event was relatively thorough in the study area because the other micaschist samples taken at and south of Jurišna Vas show the same deformational fabrics. This event is assigned to the early Tertiary event (before or at the pressure peak) as Ph_2 in the fine-grained mica layers, being parallel to the main schistosity, can show higher Si and significantly lower Na contents than those of Ph_1 (Figure 6b,d).

Again, we suggest a nearly isothermal exhumation path also due to the decrease in the Si content in Ph_2. According to the cluster of the lowest Si contents in Ph_2 (3.13 pfu) the minimum pressure reached during the recorded exhumation might be ~9.5 kbar. Such a Tertiary *P–T* loop through conditions of eclogite facies metamorphism is unusual for Austroalpine nappes. Only blueschist metamorphism (e.g. 8–10.5 kbar ~350°C, Dingeldey et al., 1997) was reported for such nappes. However, in the structurally lower Penninic unit, which is exposed, for instance, in the Tauern Window (Figure 1b), eclogite and micaschist formed at similar peak *P–T* conditions of 17–24 kbar and ≤ 635°C (Dachs & Proyer, 2002; Holland, 1979; Hoschek, 2004; Hoschek et al., 2010; Spear & Franz, 1986; Stöckhert et al., 1997). This metamorphism in the Tauern Window occurred in Eocene–Early Oligocene times (<45–31 Ma, Thöni, 2006). This time interval could be compatible with our Tertiary monazite ages because (a) the older population (48 Ma) had formed before garnet, discernable by high Y contents in monazite, and, thus, on the prograde *P–T* path and (b) the younger population (26 Ma) probably refers to the early exhumation path (see above) instead of the metamorphic peak pressure.

7.4 | Tectonic considerations

The here presented Eo-Alpine *P–T* path for metapelite with a peak pressure ~16 kbar at temperatures above 600°C (Figure 14) does not support inferences, for instance those by Janák et al. (2015), that eclogite, garnet peridotite and enclosing gneiss from the southeastern Pohorje Mts. were subjected to similar UHP conditions and coherent during the peak-pressure stage and subsequent exhumation. This postulated

coherency would also not match if the Pohorje eclogites would have experienced only 18–25 kbar and 630–750°C as reported by Miller et al. (2005) and Sassi et al. (2004). A similar peak-pressure contrast results from studies of micaschist (Schulz, 2017:15 kbar at 700°C) and eclogites (23–24 kbar at 640–690°C: e.g. Schorn & Stüwe, 2016) of the Eclogite Unit in the Saualpe area. It also means that the invoked peak-pressure contrast between the eclogite-bearing units of the Pohorje and Koralpe–Saualpe terrane and the overlying Plankogel unit (or Micaschist Unit—see Schulz, 2017) with peak pressures of 12–14 kbar at 550–580°C (Schorn & Stüwe, 2016) or ~10 kbar (Herg & Stüwe, 2018) is significantly less than original thought (Schorn & Stüwe, 2016) because the country-rocks (metasediments) determine the corresponding peak pressure and not the minor eclogite bodies in them (see also Section 7.3.2).

Another interesting tectonic aspect is the newly found Palaeogene HP event that has no room in previous tectonic models for the Pohorje Mts. and the Koralpe–Saualpe terrane (e.g. Kirst et al., 2010; Sandmann et al., 2016; Vrabec et al., 2012). The question arises why this event was not detected earlier although a thorough review of the recent literature on the here relevant area shows that indications for an event postdating the Eo-Alpine metamorphism already appear in this literature. For instance, Herg and Stüwe (2018) noted that in micaschist from the Plankogel Unit and the Pohorje Mts. two white mica generations occur similarly as in sample 16Slo12. However, these authors seem to have determined only the composition of the earlier coarser-grained generation because it was assigned to the Eo-Alpine event. Monazite ages significantly younger than Eo-Alpine were already determined (Schulz, 2017: several ages younger than 50 Ma) but according to large errors assigned to the Eo-Alpine event. The consequence of the Palaeogene HP event should be that the extrusion of Austroalpine HP nappes after intracontinental subduction, invoked by Schorn and Stüwe (2016) and Herg and Stüwe (2018), occurred in the Palaeogene and not during the Eo-Alpine.

8 | CONCLUSIONS

Four monazite generations were observed in micaschist from the Pohorje Mts. with ages of 284, 94, 48 and 26 Ma (Figure 9), which record Permian, Eo-Alpine and two Tertiary events respectively. Eclogite facies metamorphism was reconstructed based on both Eo-Alpine relics of coarse-grained phengite (3.22 Si pfu, Figure 6) and Tertiary small garnet+late fine-grained phengite (3.27 Si pfu) leading to peak-pressure conditions ~16 kbar at temperatures most likely in the range 630–645°C and 18.5–23 kbar below 600°C respectively (Figure 13). The Permian *P–T* conditions of 7.5–10 kbar at 600–650°C, obtained on inclusion minerals in porphyroblastic garnet, are compatible with a previously proposed regional Permian HT–LP event in the Austroalpine realm. However, the Eo-Alpine eclogite facies metamorphism ($P \leq 18$ kbar) is incompatible with the previously reported idea that eclogite, garnet peridotite and enclosing gneiss were subjected to similar UHP conditions, being coherent during the peak-pressure stage and subsequent exhumation (Janák et al., 2015). It could be that eclogite and peridotite had experienced UHP conditions but other rock types do not show clear evidence for such high pressures. According to Massonne (2012) and Massonne and Li (2020), the resulting pressure contrast can be explained by the accumulation of rocks such as eclogites previously exhumed in a subduction channel and those (metasediments, gneisses, etc.) deeply buried due to colliding plates. Both HP–UHP eclogites and HP metasediments and gneisses were then exhumed together in an exhumation channel and/or by surficial erosion. However, the deduced Palaeogene eclogite facies metamorphism, which is known for the Penninic units of the Eastern Alps but was identified for the Pohorje Mts. for the first time, requires a more complex geotectonic scenario for the Tertiary.

The decryption of the above described polymetamorphism of the Pohorje HP micaschist was only possible by a combination of a geochronological study of monazite in different textural settings (Section 5) and detailed evaluation of the chemical variability of the rock-forming minerals (Section 4), including their textural positions, followed by pseudosection (Section 6.2) and garnet growth and intracrystalline cation-diffusion (Section 6.4) modelling. Such studies are required to be applied to other basement regions of the Eastern Alps in order to fully understand the evolution of this orogen.

ACKNOWLEDGEMENTS

We thank Thomas Theye, Moritz Schmelz, Gisela Kwiatkowski, Matthias Leiss and Tillmann Viefhaus (all at Universität Stuttgart) for analytical assistance. The study was supported by the National Natural Science Foundation of China (no. 42002068), the MOST Special Fund from the State Key Laboratory of GPMR and the 111 Project (BP0719022). Our manuscript benefitted from critical comments by Fred Gaidies (Ottawa), an anonymous reviewer and editor Simon Harley (Edinburgh). Open access funding was enabled and organized by Projekt DEAL.

ORCID

Botao Li https://orcid.org/0000-0003-4851-8928
Hans-Joachim Massonne https://orcid.org/0000-0002-2826-4767

REFERENCES

Altherr, R., Lugovic, B., Meyer, H.-P., & Majer, V. (1995). Early Miocene post-collisional calc-alkaline-magmatism along the

easternmost segment of the Periadriatic fault system (Slovenia and Croatia). *Mineralogy and Petrology*, *54*, 225–247. https://doi.org/10.1007/BF01162863

Bernhardt, H.-J. (2007). Mincalc–v5, a software tool for mineral analyses data processing. *Acta Microscopica*, *16*, 43–44.

Braga, R., Massonne, H.-J., & Morten, L. (2007). An early metamorphic stage for the Variscan Ulten Zone gneiss (NE Italy): Evidence from mineral inclusions in kyanite. *Mineralogical Magazine*, *71*, 691–702. https://doi.org/10.1180/minmag.2007.071.6.691

Brandelik, A. (2009). CALCMIN—An EXCEL$_{TM}$ Visual Basic application for calculating mineral structural formulae from electron microprobe analyses. *Computers and Geosciences*, *35*, 1540–1551.

Brouwer, F. M., Burri, T., Engi, M., & Berger, A. (2005). Eclogite relics in the Central Alps: PT–evolution, Lu–Hf ages and implications for formation of tectonic mélange zones. *Schweizerische Mineralogische und Petrographische Mitteilungen*, *85*, 147–174.

Castro, A. E., & Spear, F. S. (2017). Reaction overstepping and re-evaluation of the peak P-T conditions of the blueschist unit Sifnos, Greece: implications for the Cyclades subduction zone. *International Geology Review*, *59*, 548–562.

Chopin, C. (1984). Coesite and pure pyrope in high–grade blueschists of the Western Alps: A first record and some consequences. *Contributions to Mineralogy and Petrology*, *86*, 107–118. https://doi.org/10.1007/BF00381838

Compagnoni, R., & Rolfo, F. (2003). Reviews of representative UHPM terranes: The Western Alps. In: D. A. Carswell & R. Compagnoni (Eds.), *Ultrahigh pressure metamorphism*. European Mineralogical Union, Notes in Mineralogy, 5, 13–50.

Connolly, J. A. D. (2005). Computation of phase equilibria by linear programming: A tool for geodynamic modeling and its application to subduction zone decarbonation. *Earth and Planetary Science Letters*, *236*, 524–541. https://doi.org/10.1016/j.epsl.2005.04.033

Dachs, E., & Proyer, A. (2002). Constraints on the duration of high-pressure metamorphism in the Tauern Window from diffusion modelling of discontinuous growth zones in eclogite garnet. *Journal of Metamorphic Geology*, *20*, 769–780. https://doi.org/10.1046/j.1525-1314.2002.00404.x

Dal Piaz, G. V., Bistacchi, A., & Massironi, M. (2003). Geological outline of the Alps. *Episodes*, *26*, 175–180. https://doi.org/10.18814/epiiugs/2003/v26i3/004

Dale, J., Holland, T., & Powell, R. (2000). Hornblende-garnet-plagioclase thermobarometry: A natural assemblage calibration of the thermodynamics of hornblende. *Contributions to Mineralogy and Petrology*, *140*, 353–362. https://doi.org/10.1007/s004100000187

Day, H. (2012). A revised diamond-graphite transition curve. *American Mineralogist*, *97*, 52–62. https://doi.org/10.2138/am.2011.3763

De Hoog, J. C., Janák, M., Vrabec, M., & Froitzheim, N. (2009). Serpentinised peridotites from an ultrahigh-pressure terrane in the Pohorje Mts. (Eastern Alps, Slovenia): Geochemical constraints on petrogenesis and tectonic setting. *Lithos*, *109*, 209–222. https://doi.org/10.1016/j.lithos.2008.05.006

Dingeldey, C., Dallmeyer, R. D., Koller, F., & Massonne, H.-J. (1997). P-T-t history of the Lower Austroalpine Nappe Complex in the ''Tarntaler Berge'' NW of the Tauern Window: Implications for the geotectonic evolution of the central Eastern Alps. *Contributions to Mineralogy and Petrology*, *129*, 1–19. https://doi.org/10.1007/s004100050319

Farré-de-Pablo, J., Proenza, J. A., González-Jiménez, J. M., Garcia-Casco, A., Colás, V., Roqué-Rossell, J., Camprubí, A., & Sánchez-Navas, A. (2019). A shallow origin for diamonds in ophiolitic chromitites. *Geology*, *47*(1), 75–78.. http://dx.doi.org/10.1130/g45640.1.

Fodor, L. I., Gerdes, A., Dunkl, I., Koroknai, B., Pécskay, Z., Trajanova, M., Horváth, P., Vrabec, M., Jelen, B., Balogh, K., & Frisch, W. (2008). Miocene emplacement and rapid cooling of the Pohorje pluton at the Alpine-Pannonian-Dinaridic junction, Slovenia. *Swiss Journal of Geosciences*, *101*, 255–271. https://doi.org/10.1007/s00015-008-1286-9

Fodor, L., Jelen, B., Márton, E., Zupancic, N., Trajanova, M., Rifelj, H., & Dunkl, I. (2002). Connection of Neogene basin formation, magmatism and cooling of metamorphics in NE Slovenia. *Geologica Carpathica*, *53*, 199–201.

Froitzheim, N., Pleuger, J., Roller, S., & Nagel, T. (2003). Exhumation of high- and ultrahigh-pressure metamorphic rocks by slab extraction. *Geology*, *31*, 925–928. https://doi.org/10.1130/G19748.1

Fuhrman, M. L., & Lindsley, D. H. (1988). Ternary-feldspar modeling and thermometry. *American Mineralogist*, *73*, 201–215.

Gaidies, F., De Capitani, C., Abart, R., & Schuster, R. (2008). Prograde garnet growth along complex P–T–t paths: Results from numerical experiments on polyphase garnet from the Wölz Complex (Austroalpine basement). *Contributions to Mineralogy and Petrology*, *155*, 673–688. https://doi.org/10.1007/s00410-007-0264-y

Habler, G., & Thöni, M. (2001). Preservation of Permo-Triassic low-pressure assemblages in the Cretaceous high-pressure metamorphic Saualpe crystalline basement (Eastern Alps, Austria). *Journal of Metamorphic Geology*, *19*, 679–697. https://doi.org/10.1046/j.0263-4929.2001.00338.x

Hacker, B. R., Kylander-Clark, A. R., Holder, R., Andersen, T. B., Peterman, E. M., Walsh, E. O., & Munnikhuis, J. K. (2015). Monazite response to ultrahigh-pressure subduction from U–Pb dating by laser ablation split stream. *Chemical Geology*, *409*, 28–41. https://doi.org/10.1016/j.chemgeo.2015.05.008

Hauzenberger, C. A., Taferner, H., & Konzett, J. (2016). Genesis of chromium-rich kyanite in eclogite-facies Cr-spinel-bearing gabbroic cumulates, Pohorje Massif, Eastern Alps. *American Mineralogist*, *101*, 448–460. https://doi.org/10.2138/am-2016-5178

Henry, D. J., Guidotti, C. V., & Thomson, J. A. (2005). The Ti–saturation surface for low-to-medium pressure metapelitic biotites: Implications for geothermometry and Ti-substitution mechanisms. *American Mineralogist*, *90*, 316–328. https://doi.org/10.2138/am.2005.1498

Herg, A., & Stüwe, K. (2018). Tectonic interpretation of the metamorphic field gradient south of the Koralpe in the Eastern Alps. *Austrian Journal of Earth Sciences*, *111*(2), 155–170. https://doi.org/10.17738/ajes.2018.0010

Hermann, J., & Rubatto, D. (2003). Relating zircon and monazite domains to garnet growth zones: Age and duration of granulite facies metamorphism in the Val Malenco lower crust. *Journal of Metamorphic Geology*, *21*, 833–852. https://doi.org/10.1046/j.1525-1314.2003.00484.x

Hoisch, T. D., Wells, M. L., & Grove, M. (2008). Age trends in garnet hosted monazite inclusions from upper amphibolite facies schist in the northern Grouse Creek Mountains, Utah. *Geochimica et Cosmochimica Acta*, *72*, 5505–5520. https://doi.org/10.1016/j.gca.2008.08.012

Holland, T. J. B. (1979). High water activities in the generation of high pressure kyanite eclogites of the Tauern Window, Austria. *The Journal of Geology*, *87*, 1–27. https://doi.org/10.1086/628388

Holland, T., Baker, J. M., & Powell, R. (1998). Mixing properties and activity-composition relationships of chlorites in the system MgO-FeO-Al_2O_3-SiO_2-H_2O. *European Journal of Mineralogy*, *10*, 395–406. https://doi.org/10.1127/ejm/10/3/0395

Holland, T., & Powell, R. (1991). A compensated-Redlich-Kwong (CORK) equation for volumes and fugacities of CO_2 and H_2O in the range 1 bar to 50 kbar and 100–1600ºC. *Contributions to Mineralogy and Petrology*, *109*, 265–273.

Holland, T., & Powell, R. (1996). Thermodynamics of order-disorder in minerals: II. Symmetric formalism applied to solid solutions. *American Mineralogist*, *81*, 1425–1437. https://doi.org/10.2138/am-1996-11-1215

Holland, T. J. B., & Powell, R. (1998). An internally consistent thermodynamic data set for phases of petrological interest. *Journal of Metamorphic Geology*, *16*, 309–343. https://doi.org/10.1111/j.1525-1314.1998.00140.x

Holland, T., & Powell, R. (2001). Calculation of phase relations involving haplogranitic melts using an internally consistent thermodynamic dataset. *Journal of Petrology*, *42*, 673–683.

Holland, T. J. B., & Powell, R. (2011). An improved and extended internally-consistent thermodynamic dataset for phases of petrological interest, involving a new equation of state for solids. *Journal of Metamorphic Geology*, *29*, 333–383. https://doi.org/10.1111/j.1525-1314.2010.00923.x

Hoschek, G. (2004). Comparison of calculated P–T pseudosections for a kyanite eclogite from the Tauern Window, Eastern Alps, Austria. *European Journal of Mineralogy*, *16*, 59–72. https://doi.org/10.1127/0935-1221/2004/0016-0059

Hoschek, G., Konzett, J., & Tessadri, R. (2010). Phase equilibria in quartzitic garnet-kyanite-chloritoid micaschist from the Eclogite Zone, Tauern Window, Eastern Alps. *European Journal of Mineralogy*, *22*, 721–732. https://doi.org/10.1127/0935-1221/2010/0022-2049

Hurai, V., Janák, M., & Thomas, R. (2010). Fluid–assisted retrogression of garnet and P-T history of metapelites from HP/UHP metamorphic terrane (Pohorje Mountains, Eastern Alps). *Contributions to Mineralogy and Petrology*, *160*, 203–218. https://doi.org/10.1007/s00410-009-0473-7

Janák, M., Cornell, D., Froitzheim, N., De Hoog, J. C., Broska, I., Vrabec, M., & Hurai, V. (2009). Eclogite-hosting metapelites from the Pohorje Mountains (Eastern Alps): P-T evolution, zircon geochronology and tectonic implications. *European Journal of Mineralogy*, *21*, 1191–1212. https://doi.org/10.1127/0935-1221/2009/0021-1966

Janák, M., Froitzheim, N., Lupták, B., Vrabec, M., & Ravna, E. J. K. (2004). First evidence for ultrahigh-pressure metamorphism of eclogites in Pohorje, Slovenia: Tracing deep continental subduction in the Eastern Alps. *Tectonics*, *23*, TC5014. https://doi.org/10.1029/2004TC001641

Janák, M., Froitzheim, N., Vrabec, M., Krogh Ravna, E. J., & De Hoog, J. C. M. (2006). Ultrahigh-pressure metamorphism and exhumation of garnet peridotite in Pohorje, Eastern Alps. *Journal of Metamorphic Geology*, *24*, 19–31. https://doi.org/10.1111/j.1525-1314.2005.00619.x

Janák, M., Froitzheim, N., Yoshida, K., Sasinková, V., Nosko, M., Kobayashi, T., Hirajima, T., & Vrabec, M. (2015). Diamond in metasedimentary crustal rocks from Pohorje, Eastern Alps: A window to deep continental subduction. *Journal of Metamorphic Geology*, *33*, 495–512. https://doi.org/10.1111/jmg.12130

Janots, E., Berger, A., Gnos, E., Whitehouse, M., Lewin, E., & Pettke, T. (2012). Constraints on fluid evolution during metamorphism from U-Th-Pb systematics in Alpine hydrothermal monazite. *Chemical Geology*, *326*, 61–71. https://doi.org/10.1016/j.chemgeo.2012.07.014

Kirst, F., Sandmann, S., Nagel, T., Froitzheim, N., & Janák, M. (2010). Tectonic evolution of the southeastern part of the Pohorje Mountains (Eastern Alps, Slovenia). *Geologica Carpathica*, *61*, 451–461. https://doi.org/10.2478/v10096-010-0027-y

Kohn, M. J., Wieland, M. S., Parkinson, C. D., & Upreti, B. N. (2005). Five generations of monazite in Langtang gneisses: Implications for chronology of the Himalayan metamorphic core. *Journal of Metamorphic Geology*, *23*, 399–406. https://doi.org/10.1111/j.1525-1314.2005.00584.x

Konrad–Schmolke, M., O'Brien, P. J., de Capitani, C., & Carswell, D. A. (2008). Garnet growth at high- and ultra-high pressure conditions and the effect of element fractionation on mineral modes and composition. *Lithos*, *103*, 309–332. https://doi.org/10.1016/j.lithos.2007.10.007

Krenn, E., Janák, M., Finger, F., Broska, I., & Konečný, P. (2009). Two types of metamorphic monazite with contrasting La/Nd, Th, and Y signatures in an ultrahigh-pressure metapelite from the Pohorje Mountains, Slovenia: Indications for pressure-dependent REE exchange between apatite and monazite? *American Mineralogist*, *94*, 801–815. https://doi.org/10.2138/am.2009.2981

Krenn, E., Schulz, B., & Finger, F. (2012). Three generations of monazite in Austroalpine basement rocks to the south of the Tauern Window: Evidence for Variscan, Permian and Eo-Alpine metamorphic events. *Swiss Journal of Geosciences*, *105*, 343–360. https://doi.org/10.1007/s00015-012-0104-6

Li, B., & Massonne, H.-J. (2016). Early Variscan P–T evolution of an eclogite body and adjacent orthogneiss from the northern Malpica–Tuy shear-zone in NW Spain. *European Journal of Mineralogy*, *28*, 1131–1154. https://doi.org/10.1127/ejm/2016/0028-2569

Li, B., & Massonne, H.-J. (2017). Contrasting metamorphic evolution of metapelites from the Malpica–Tuy unit and the underlying so-called parautochthon at the coast of NW Spain. *Lithos*, *286*, 92–108. https://doi.org/10.1016/j.lithos.2017.06.003

Li, B., & Massonne, H.-J. (2018). Two Tertiary metamorphic events recognized in high-pressure metapelites of the Nevado–Filábride Complex (Betic Cordillera, S Spain). *Journal of Metamorphic Geology*, *36*, 603–630. https://doi.org/10.1111/jmg.12312

Li, B., Massonne, H.-J., & Opitz, J. (2017). Clockwise and anticlockwise P-T paths of high-pressure rocks from the 'La Pioza' eclogite body of the Malpica-Tuy Complex, NW Spain. *Journal of Petrology*, *58*, 1363–1392. https://doi.org/10.1093/petrology/egx057

Li, B., Massonne, H.-J., & Zhang, J.-F. (2020). Evolution of a gneiss in the Seve nappe complex of central Sweden – Hints at an early Caledonian, medium-pressure metamorphism. *Lithos*, *376–377*, 105746.

Lo Pò, D., Braga, R., Massonne, H.-J., Molli, G., Montanini, A., & Theye, T. (2016). Fluid-induced breakdown of monazite in medium-grade metasedimentary rocks of the Pontremoli basement (Northern Apennines, Italy). *Journal of Metamorphic Geology*, *34*, 63–84. https://doi.org/10.1111/jmg.12171

Ludwig, K. R. (2003). ISOPLOT/Ex Version 3.00, a geochronological toolkit for Microsoft Excel. *Berkeley Geochronology Center Special Publication*, *4*, 1–71.

Massonne, H.-J. (1999). Experimental aspects of UHP metamorphism in pelitic systems. *International Geology Review*, *41*, 623–638. https://doi.org/10.1080/00206819909465162

Massonne, H.-J. (2010). Phase relations and dehydration behaviour of calcareous sediments at very-low to low grade metamorphic conditions. *Periodico di Mineralogia*, *79*, 21–43.

Massonne, H.-J. (2012). Formation of amphibole and clinozoisite-epidote in eclogite owing to fluid infiltration during exhumation in a subduction channel. *Journal of Petrology*, *53*, 1969–1998. https://doi.org/10.1093/petrology/egs040

Massonne, H.-J. (2013). Constructing the pressure-temperature path of ultrahigh-pressure rocks. *Elements*, *9*, 267–272. https://doi.org/10.2113/gselements.9.4.267

Massonne, H.-J. (2014). Wealth of P-T-t information in medium-high grade metapelites: Example from the Jubrique Unit of the Betic Cordillera, S Spain. *Lithos*, *208*, 137–157. https://doi.org/10.1016/j.lithos.2014.08.027

Massonne, H.-J. (2016). Tertiary high-pressure metamorphism recorded in andalusite-bearing mica-schist, southern Pirin Mts. SW Bulgaria. *European Journal of Mineralogy*, *28*, 1187–1202. https://doi.org/10.1127/ejm/2016/0028-2575

Massonne, H.-J. (2019). Forum comment: A shallow origin for diamonds in ophiolitic chromitites. *Geology*, *47*, e476.

Massonne, H.-J., Barr, S. M., White, C. E., & Miller, B. V. (2018). The Pocologan metamorphic suite of southern New Brunswick, Canada: New constraints on age and conditions of medium- to high-pressure metamorphism. *Tectonophysics*, *747–748*, 177–190.

Massonne, H.-J., Cruciani, G., Franceschelli, M., & Musumeci, G. (2018). Anti-clockwise pressure-temperature paths record Variscan upper-plate exhumation: Example from micaschists of the Porto Vecchio region, Corsica. *Journal of Metamorphic Geology*, *36*, 55–77. https://doi.org/10.1111/jmg.12283

Massonne, H.-J., & Li, B. (2020). Zoning of eclogitic garnet cores – A key pattern demonstrating the dominance of tectonic erosion as part of the burial process of worldwide occurring eclogites. *Earth-Science Reviews*, *210*, 103356. https://doi.org/10.1016/j.earscirev.2020.103356

Massonne, H.-J., & Toulkeridis, T. (2012). Widespread relics of high-pressure metamorphism confirm major terrane accretion in Ecuador: A new example from the Northern Andes. *International Geology Review*, *54*, 67–80. https://doi.org/10.1080/00206814.2010.498907

Massonne, H.-J., & Willner, A. P. (2008). Phase relations and dehydration behaviour of psammopelite and mid-ocean ridge basalt at very-low-grade to low-grade metamorphic conditions. *European Journal of Mineralogy*, *20*, 867–879. https://doi.org/10.1127/0935-1221/2008/0020-1871

Michard, A., Chopin, C., & Henry, C. (1993). Compression versus extension in the exhumation of the Dora–Maira coesite-bearing unit, Western Alps, Italy. *Tectonophysics*, *221*, 173–193. https://doi.org/10.1016/0040-1951(93)90331-D

Miller, C., & Konzett, J. (2005). Comment on "First evidence for ultrahigh–pressure metamorphism of eclogites in Pohorje Slovenia: Tracing deep continental subduction in the eastern Alps" by Marian Janák et al. *Tectonics*, *24*(6), TC6010. https://doi.org/10.1029/2004TC001765

Miller, C., Mundil, R., Thöni, M., & Konzett, J. (2005). Refining the timing of eclogite metamorphism: A geochemical, petrological, Sm–Nd and U–Pb case study from the Pohorje Mountains, Slovenia (Eastern Alps). *Contributions to Mineralogy and Petrology*, *150*, 70–84. https://doi.org/10.1007/s00410-005-0004-0

Miller, C., & Thöni, M. (1997). Eo-Alpine eclogitisation of Permian MORB-type gabbros in the Koralpe (Eastern Alps, Austria): New geochronological, geochemical and petrological data. *Chemical Geology*, *137*, 283–310. https://doi.org/10.1016/S0009-2541(96)00165-9

Morauf, W. (1981). Rb-Sr und K-Ar-Isotopen-Alter an Pegmatiten aus Kor-und Saualpe, SE-Ostalpen, Österreich. *Tschermaks Mineralogische Und Petrographische Mitteilungen*, *28*, 113–129.

Mottram, C. M., Warren, C. J., Regis, D., Roberts, N. M., Harris, N. B., Argles, T. W., & Parrish, R. R. (2014). Developing an inverted Barrovian sequence: Insights from monazite petrochronology. *Earth and Planetary Science Letters*, *403*, 418–431. https://doi.org/10.1016/j.epsl.2014.07.006

Neubauer, F., Genser, J., & Handler, R. (2000). The Eastern Alps: Result of a two–stage collision process. *Mitteilungen der Österreichischen Geologischen Gesellschaft*, *92*, 117–134.

Perchuk, A. L., Burchard, M., Schertl, H.-P., Maresch, W. V., Gerya, T. V., Bernhard, H.-J., & Vidal, O. (2009). Diffusion of divalent cations in garnet: Multi-couple experiments. *Contributions to Mineralogy and Petrology*, *157*, 573–592. https://doi.org/10.1007/s00410-008-0353-6

Perchuk, A. L., & Gerya, T. V. (2005). Subsidence and exhumation dynamics of eclogites in the Yukon-Tanana Terrane, Canadian Cordillera: Petrological reconstructions and geodynamic modeling. *Petrology*, *13*, 253–266.

Powell, R., & Holland, T. (1999). Relating formulations of the thermodynamics of mineral solid solutions: Activity modeling of pyroxenes, amphiboles, and micas. *American Mineralogist*, *84*, 1–14. https://doi.org/10.2138/am-1999-1--201

Pujol-Solà, N., Garcia-Casco, A., Proenza, J. A., González-Jiménez, J. M., del Campo, A., Colás, V., Canals, À., Sánchez-Navas, A., & Roqué-Rosell, J. (2020). Diamond forms during low pressure serpentinisation of oceanic lithosphere. *Geochemical Perspectives Letters*, 19–24. http://dx.doi.org/10.7185/geochemlet.2029

Pyle, J. M., & Spear, F. S. (2003). Four generations of accessory phase growth in low pressure migmatites from SW New Hampshire. *American Mineralogist*, *88*, 338–351. https://doi.org/10.2138/am-2003-2-311

Pyle, J. M., Spear, F. S., Rudnick, R. L., & McDonough, W. F. (2001). Monazite-xenotime-garnet equilibrium in metapelites and a new monazite-garnet thermometer. *Journal of Petrology*, *42*, 2083–2107. https://doi.org/10.1093/petrology/42.11.2083

Rahimi, G., & Massonne, H.-J. (2018). Pressure–temperature–time evolution of a Variscan garnet-bearing micaschist from the northern Fichtelgebirge, NW Bohemian Massif in central Europe. *Lithos*, *316–317*, 366–384.

Ratschbacher, L., Frisch, W., Neubauer, F., Schmid, S. M., & Neugebauer, J. (1989). Extension in compressional orogenic belts: The eastern Alps. *Geology*, *17*, 404–407. https://doi.org/10.1130/0091-7613(1989)017<0404:EICOBT>2.3.CO;2

Regis, D., Warren, C. J., Mottram, C. M., & Roberts, N. M. W. (2016). Using monazite and zircon petrochronology to constrain the P–T–t evolution of the middle crust in the Bhutan Himalaya. *Journal of Metamorphic Geology*, *34*, 617–639.

Reinecke, T. (1998). Prograde high–to ultrahigh–pressure metamorphism and exhumation of oceanic sediments at Lago di Cignana, Zermatt–Saas Zone, western Alps. *Lithos*, *42*, 147–189. https://doi.org/10.1016/S0024-4937(97)00041-8

Rubatto, D., Hermann, J., & Buick, I. S. (2006). Temperature and bulk composition control on the growth of monazite and zircon during low-pressure anatexis (Mount Stafford, central Australia). *Journal of Petrology*, *47*, 1973–1996. https://doi.org/10.1093/petrology/egl033

Sachsenhofer, R. F., Dunkl, I., Hasenhüttl, C., & Jelen, B. (1998). Miocene thermal history of the southwestern margin of the Styrian Basin: Vitrinite reflectance and fission–track data from the Pohorje/Kozjak area (Slovenia). *Tectonophysics*, *297*, 17–29. https://doi.org/10.1016/S0040-1951(98)00161-9

Sandmann, S., Herwartz, D., Kirst, F., Froitzheim, N., Nagel, T. J., Fonseca, R. O. C., Münker, C., & Janák, M. (2016). Timing of eclogite–facies metamorphism of mafic and ultramafic rocks from the Pohorje Mountains(Eastern Alps, Slovenia) based on Lu–Hf garnet geochronometry. *Lithos*, *262*, 576–585. https://doi.org/10.1016/j.lithos.2016.08.002

Sassi, R., Mazzoli, C., Miller, C., & Konzett, J. (2004). Geochemistry and metamorphic evolution of the Pohorje Mountain eclogites from the easternmost Austroalpine basement of the Eastern Alps (Northern Slovenia). *Lithos*, *78*, 235–261. https://doi.org/10.1016/j.lithos.2004.05.002

Schmid, S. M., Fügenschuh, B., Kissling, E., & Schuster, R. (2004). Tectonic map and overall architecture of the Alpine orogeny. *Eclogae Geologicae Helvetiae*, *97*, 93–117. https://doi.org/10.1007/s00015-004-1113-x

Schorn, S., & Stüwe, K. (2016). The Plankogel detachment of the Eastern Alps: Petrological evidence for an orogen–scale extraction fault. *Journal of Metamorphic Geology*, *34*, 147–166. https://doi.org/10.1111/jmg.12176

Schulz, B. (2017). Polymetamorphism in garnet micaschists of the Saualpe Eclogite Unit (Eastern Alps, Austria), resolved by automated SEM methods and EMP-Th-U-Pb monazite dating. *Journal of Metamorphic Geology*, *35*, 141–163. https://doi.org/10.1111/jmg.12224

Schuster, R., Scharbert, S., Abart, R., & Frank, W. (2001). Permo–Triassic extension and related HT/LP metamorphism in the Austroalpine–Southalpine realm. *Mitteilungen der Geologie und Bergbau Studenten Österreichs*, *44*, 111–141.

Schuster, R., & Stüwe, K. (2008). Permian metamorphic event in the Alps. *Geology*, *36*, 603–606. https://doi.org/10.1130/G24703A.1

Seydoux–Guillaume, A.-M., Montel, J.-M., Bingen, B., Bosse, V., de Parseval, P., Paquette, J.-L., Janots, E., & Wirth, R. (2012). Low-temperature alteration of monazite: Fluid mediated coupled dissolution-precipitation, irradiation damage, and disturbance of the U-Pb and Th-Pb chronometers. *Chemical Geology*, *330*, 140–158. https://doi.org/10.1016/j.chemgeo.2012.07.031

Smye, A. J., Greenwood, L. V., & Holland, T. J. B. (2010). Garnet-chloritoid-kyanite assemblages: Eclogite facies indicators of subduction constraints in orogenic belts. *Journal of Metamorphic Geology*, *28*, 753–768. https://doi.org/10.1111/j.1525-1314.2010.00889.x

Spear, F. S. (2010). Monazite–allanite phase relations in metapelites. *Chemical Geology*, *279*, 55–62. https://doi.org/10.1016/j.chemgeo.2010.10.004

Spear, F. S. (2017). Garnet growth after overstepping. *Chemical Geology*, *466*, 491–499. https://doi.org/10.1016/j.chemgeo.2017.06.038

Spear, F. S., & Franz, G. (1986). P–T evolution of metasediments from the Eclogite Zone, south-central Tauern Window, Austria. *Lithos*, *19*, 219–234. https://doi.org/10.1016/0024-4937(86)90024-1

Spear, F. S., Thomas, J. B., & Hallett, B. W. (2014). Overstepping the garnet isograd: A comparison of QuiG barometry and thermodynamic modeling. *Contributions to Mineralogy and Petrology*, *168*(3), Article No. 1059, 15 p.

Štípská, P., Chopin, F., Skrzypek, E., Schulmann, K., Pitra, P., Lexa, O., Martelat, J. E., Bollinger, C., & Žáčková, E. (2012). The juxtaposition of eclogite and mid-crustal rocks in the Orlica-Śnieżnik Dome, Bohemian Massif. *Journal of Metamorphic Geology*, *30*, 213–234. https://doi.org/10.1111/j.1525-1314.2011.00964.x

Štípská, P., & Powell, R. (2005). Constraining the P–T path of a MORB-type eclogite using pseudosections, garnet zoning and garnet-clinopyroxene thermometry: An example from the Bohemian Massif. *Journal of Metamorphic Geology*, *23*, 725–743. https://doi.org/10.1111/j.1525-1314.2005.00607.x

Stöckhert, B., Massonne, H.-J., & Nowlan, E. U. (1997). Low differential stress during high-pressure metamorphism: The microstructural record of a metapelite from the Eclogite Zone, Tauern Window, Eastern Alps. *Lithos*, *41*, 103–118.

Stüwe, K., & Schuster, R. (2010). Initiation of subduction in the Alps: Continent or ocean? *Geology*, *38*, 175–178.

Tajčmanová, L., Connolly, J. A. D., & Cesare, B. (2009). A thermodynamic model for titanium and ferric iron solution in biotite. *Journal of Metamorphic Geology*, *27*, 153–165.

Tenczer, V., Powell, R., & Stüwe, K. (2006). Evolution of H_2O content in a polymetamorphic terrane: The Plattengneiss Shear Zone (Koralpe, Austria). *Journal of Metamorphic Geology*, *24*, 281–295.

Thöni, M. (2003). Sm-Nd isotope systematics in garnet from different lithologies (Eastern Alps): Age results, and an evaluation of potential problems for garnet Sm-Nd chronometry. *Chemical Geology*, *194*, 353–379.

Thöni, M. (2006). Dating eclogite-facies metamorphism in the Eastern Alps – Approaches, results, interpretations: A review. *Mineralogy and Petrology*, *88*, 123–148.

Thöni, M., & Jagoutz, E. (1992). Some new aspects of dating eclogites in orogenic belts: Sm-Nd, Rb-Sr, and Pb-Pb isotopic results from the Austroalpine Saualpe and Koralpe type-locality (Carinthia/Styria, southeastern Austria). *Geochimica et Cosmochimica Acta*, *56*, 347–368.

Thöni, M., & Miller, C. (1996). Garnet Sm-Nd data from the Saualpe and the Koralpe (Eastern Alps, Austria): Chronological and P-T constraints on the thermal and tectonic history. *Journal of Metamorphic Geology*, *14*, 453–466.

Thöni, M., & Miller, C. (2009). The "Permian event" in the Eastern European Alps: Sm-Nd and P-T data recorded by multi-stage garnet from the Plankogel unit. *Chemical Geology*, *260*, 20–36.

Thöni, M., & Miller, C. (2010). Andalusite formation in a fast exhuming high-P wedge: Textural, microchemical, and Sm-Nd and Rb-Sr age constraints for a Cretaceous P-T-t path at Kienberg, Saualpe (Eastern Alps). *Austrian Journal of Earth Sciences*, *103*, 118–131.

Thöni, M., Miller, C., Blichert-Toft, J., Whitehouse, M. J., Konzett, J., & Zanetti, A. (2008). Timing of high-pressure metamorphism and exhumation of the eclogite type-locality (Kupplerbrunn-Prickler Halt, Saualpe, south-eastern Austria): Constraints from correlations of the Sm-Nd, Lu-Hf, U-Pb and Rb-Sr isotopic systems. *Journal of Metamorphic Geology*, *26*, 561–581. https://doi.org/10.1111/j.1525-1314.2008.00778.x

Tomkins, H. S., Powell, R., & Ellis, D. J. (2007). The pressure dependence of the zirconium-in-rutile thermometer. *Journal of Metamorphic Geology*, *25*, 703–713. https://doi.org/10.1111/j.1525-1314.2007.00724.x

Trajanova, M., Pécskay, Z., & Itaya, T. (2008). K-Ar geochronology and petrography of the Miocene Pohorje Mountains batholith, Slovenia. *Geologica Carpathica*, *59*, 247–260.

Uher, P., Janák, M., Konečný, P., & Vrabec, M. (2014). Rare-element granitic pegmatite of Miocene age emplaced in UHP rocks from Visole, Pohorje Mountains (Eastern Alps, Slovenia): Accessory minerals, monazite and uraninite chemical dating. *Geologica Carpathica*, *65*, 131–146. https://doi.org/10.2478/geoca-2014-0009

Vrabec, M., Janák, M., Froitzheim, N., & De Hoog, J. C. (2012). Phase relations during peak metamorphism and decompression of the

UHP kyanite eclogites, Pohorje Mountains (Eastern Alps, Slovenia). *Lithos*, *144*, 40–55. https://doi.org/10.1016/j.lithos.2012.04.004

Waizenhöfer, F., & Massonne, H.-J. (2017). Monazite in a Variscan mylonitic paragneiss from the Münchberg Metamorphic Complex (NE Bavaria) records Cadomian protolith ages. *Journal of Metamorphic Geology*, *35*, 453–469. https://doi.org/10.1111/jmg.12240

Wang, J. M., Rubatto, D., & Zhang, J. J. (2015). Timing of partial melting and cooling across the Greater Himalayan Crystalline Complex (Nyalam, Central Himalaya): In-sequence thrusting and its implications. *Journal of Petrology*, *56*, 1677–1702. https://doi.org/10.1093/petrology/egv050

Wei, C. J., Powell, R., & Zhang, L. F. (2003). Eclogites from the south Tianshan, NW China: Petrological characteristic and calculated mineral equilibria in the Na_2O-CaO-FeO-MgO-Al_2O_3-SiO_2-H_2O system. *Journal of Metamorphic Geology*, *21*, 163–179. https://doi.org/10.1046/j.1525-1314.2003.00435.x

White, R. W., Powell, R., & Holland, T. J. B. (2001). Calculation of partial melting equilibria in the system Na_2O-CaO-K_2O-FeO-MgO-Al_2O_3-SiO_2-H_2O (NCKFMASH). *Journal of Metamorphic Geology*, *19*, 139–153.

White, R. W., Powell, R., & Holland, T. J. B. (2007). Progress relating to calculation of partial melting equilibria for metapelites. *Journal of Metamorphic Geology*, *25*, 511–527. https://doi.org/10.1111/j.1525-1314.2007.00711.x

White, R. W., Powell, R., Holland, T. J. B., Johnson, T. E., & Green, E. C. R. (2014). New mineral activity-composition relations for thermodynamic calculations in metapelitic systems. *Journal of Metamorphic Geology*, *32*, 261–286. https://doi.org/10.1111/jmg.12071

White, R. W., Powell, R., Holland, T. J. B., & Worley, B. A. (2000). The effect of TiO_2 and Fe_2O_3 on metapelitic assemblages at greenschist and amphibolite facies conditions: Mineral equilibria calculations in the system K_2O-FeO-MgO-Al_2O_3-SiO_2-H_2O-TiO_2-Fe_2O_3. *Journal of Metamorphic Geology*, *18*, 497–511.

Whitney, D. L., & Evans, B. W. (2010). Abbreviations for names of rock–forming minerals. *American Mineralogist*, *95*, 185–187. https://doi.org/10.2138/am.2010.3371

Williams, M. L., Jercinovic, M. J., Harlov, D. E., Budzyń, B., & Hetherington, C. J. (2011). Resetting monazite ages during fluid-related alteration. *Chemical Geology*, *283*, 218–225. https://doi.org/10.1016/j.chemgeo.2011.01.019

Williams, M. L., Jercinovic, M. J., & Hetherington, C. J. (2007). Microprobe monazite geochronology: Understanding geologic processes by integrating composition and chronology. *Annual Review of Earth and Planetary Sciences*, *35*, 137–175. https://doi.org/10.1146/annurev.earth.35.031306.140228

Willner, A. P., Krohe, A., & Maresch, W. V. (2000). Interrelated P-T-t-d paths in the Variscan Erzgebirge dome (Saxony, Germany): Constraints on the rapid exhumation of high-pressure rocks from the root zone of a collisional orogeny. *International Geology Review*, *42*, 64–85. https://doi.org/10.1080/00206810009465070

Zack, T., Moraes, R., & Kronz, A. (2004). Temperature dependence of Zr in rutile: Empirical calibration of a rutile thermometer. *Contributions to Mineralogy and Petrology*, *148*, 471–488. https://doi.org/10.1007/s00410-004-0617-8

Zeh, A., Holland, T. J. B., & Klemd, R. (2005). Phase relationships in grunerite-garnet-bearing amphibolites in the system CFMASH, with applications to metamorphic rocks from the Central Zone of the Limpopo Belt, South Africa. *Journal of Metamorphic Geology*, *23*, 1–17. https://doi.org/10.1111/j.1525-1314.2005.00554.x

Supporting Information

Additional supporting information may be found online in the Supporting Information section.

Figure S1. Isopleths for molar fractions of grossular and pyrope in garnet calculated for the bulk-rock compositions XRF1 and XRF2 (Table 1) with thermodynamic data set 1.

Figure S2. *P–T* pseudosection for sample 16Slo12, calculated for bulk-rock composition XRFB1 (Table 1) with thermodynamic data set 1, and isopleths of molar fractions of grossular, pyrope and spessartine in garnet to deduce peak-pressure conditions of the Eo-Alpine stage.

Figure S3. As Figure S2 but for bulk-rock composition XRFA1 (Table 1) and thermodynamic data set 2.

Figure S4. *P–T* pseudosection for sample 16Slo12, calculated for effective bulk-rock composition BEBC (Table 1) with thermodynamic data set 1, and isopleths of molar fractions of grossular, pyrope and spessartine in garnet to deduce the Tertiary peak-pressure conditions.

Figure S5. As Figure S4 but for effective bulk-rock composition AEBC (Table 1) and thermodynamic data set 2.

Figure S6. Modal content of garnet related to the *P–T* pseudosection of Figure 10a.

Figure S7. Temperatures obtained with the Ti-in-biotite thermometer by Henry et al. (2005).

Table S1. Estimation of the original bulk-rock composition (Table 1: XRFB) of sample 16Slo12 following strategy B.

How to cite this article: Li B, Massonne H-J, Koller F, Zhang J. Metapelite from the high- to ultrahigh-pressure terrane of the Eastern Alps (Pohorje Mountains, Slovenia)—New pressure, temperature and time constraints on a polymetamorphic rock. *J Metamorph Geol*. 2020;00:1–32. https://doi.org/10.1111/jmg.12581